J. Membrane Biol. 179, 223–242 (2001)
DOI: 10.1007/s002320010049

The Journal of
Membrane
Biology

Two-Step Mechanism of Phlorizin Binding to the SGLT1 Protein in the Kidney

N. Oulianova, S. Falk, A. Berteloot
Membrane Transport Research Group, Department of Physiology, Faculty of Medicine, Université de Montréal, CP 6128, succursale "Centre-Ville", Montreal (Québec) Canada H3C 3J7

Received: 22 June 2000/Revised: 1 November 2000

Abstract. The relationships between phlorizin binding and Na^+-glucose cotransport were addressed in rabbit renal brush-border membrane vesicles. At pH 6.0 and 8.6, high affinity phlorizin binding followed single exponential kinetics. With regard to phlorizin concentrations, the binding data conformed to simple Scatchard kinetics with lower apparent affinities of onset binding (K_{di} = 12–30 μM) compared to steady-state binding (K_{de} = 2–5 μM), and the first-order rate constants demonstrated a Michaelis-Menten type of dependence with K_m values identical to K_{di}. Phlorizin dissociation from its receptor sites also followed single exponential kinetics with time constants insensitive to saturating concentrations of unlabeled phlorizin or D-glucose, but directly proportional to Na^+ concentrations. These results prove compatible with homogeneous binding to SGLT1 whereby fast Na^+ and phlorizin addition on the protein is followed by a slow conformation change preceding further Na^+ attachment, thus occluding part of the phlorizin-bound receptor complexes. This two-step mechanism of inhibitor binding invalidates the recruitment concept as a possible explanation of the fast-acting slow-binding paradigm of phlorizin, which can otherwise be resolved as follows: the rapid formation of an initial collision complex explains the fast-acting behavior of phlorizin with regard to its inhibition of glucose transport; however, because this complex also rapidly dissociates in a rapid filtration assay, the slow kinetics of phlorizin binding are only apparent and reflect its slow isomerization into more stable forms.

Key words: Transport kinetics — Inhibitor binding mechanisms — Cotransport models — Rapid filtration technique — Membrane vesicles (rabbit kidney cortex)

Correspondence to: A. Berteloot

Introduction

Turner and Moran [57, 58] brought evidence for kinetic heterogeneity of Na^+-dependent D-glucose transport (SGLT) along the rabbit proximal tubule and characterized both high-affinity (HAG) and low-affinity (LAG) glucose transport pathways in renal brush border membrane vesicles (BBMV) isolated from the outer medulla and outer cortex, respectively. When such studies are correlated with the clinical findings regarding the defects in intestinal and renal sugar absorption, it is usually assumed that HAG would represent the functional expression of renal/intestinal SGLT1 while LAG would characterize the activity of a kidney-specific gene product (SGLT2) that has yet to be cloned in the rabbit [13]. However, there is some controversy in the literature as to whether the kinetic heterogeneity observed in BBMV isolated from the kidney cortex and/or medulla is the unique and direct consequence of molecular diversity [6, 10, 23, 24, 31, 33, 44, 47, 62].

Recent studies from our group [44] confirmed the kinetic heterogeneity of SGLT in rabbit renal BBMV isolated from the whole kidney cortex and compared the functional characteristics of HAG and LAG transport *vs.* the cloned SGLT1 [45] and candidate SGLT2 [28, 39, 40, 65] systems expressed in cRNA-injected oocytes. Inconsistencies with regard to the specificity of glucose *vs.* galactose transport and the sensitivity of glucose transport to phlorizin inhibition led us to conclude that the kinetic heterogeneity observed in BBMV most likely reflects different transport properties of rabbit SGLT1 (rbSGLT1) rather than the coexpression of distinct rbSGLT1 and rbSGLT2 proteins. Alternatively, structural similarities between the two transport proteins would give them a number of overlapping functional characteristics among which the similar sensitivity of sugar transport to phlorizin inhibition (K_i = 15 μM) contrasts with the 27- and 55-fold differences in transport affinities of

rbSGLT1 and rbSGLT2 for glucose and galactose, respectively [44]. In any event, the latter results challenge Turner and Moran's view [57, 58] that high affinity (HAP) and low affinity (LAP) phlorizin binding would characterize the renal LAG and HAG transport pathways, respectively. In this respect, the experimental evidence supporting the latter concept can be seriously questioned.

First, when reevaluated to account for competitive inhibition [44], the relative potencies of phlorizin at inhibiting sugar transport at a fixed glucose concentration of 1 mM in the outer cortical and outer medullary vesicles [57] appear fully compatible with similar K_i values of 5–15 μM in the two preparations.

Second, phlorizin binding studies have not yet considered the fact that the inhibitor molecule is a weak acid with estimated pH_a values of 7.2 [18] or 7.4 [54]. Accordingly, at these physiological pH values where phlorizin binding studies are usually performed, the similar amounts of the neutral *keto-* (HPz) and negatively charged *enol-* (Pz^-) forms of the phlorizin molecule might contribute quite significantly to the observed heterogeneity of binding.

Last, as pointed out recently [20], any attempt to establish a close correspondence between glucose transport and phlorizin binding studies is complicated by the existence of the so-called fast-acting slow-binding paradigm whereby phlorizin inhibition of SGLT is fast on the steady-state time scale of 0–9 sec [44] whereas phlorizin binding to BBMV requires several minutes to reach equilibrium [2, 11, 25, 30, 49, 60]. So far, this situation has been tentatively explained according to the recruitment concept first proposed by Aronson [2] and against which the kinetics of phlorizin binding to renal and intestinal membranes have been interpreted ever since [59]. Note that this hypothesis primarily rests on circumstantial pieces of evidence [2, 29, 54, 55, 60] and assumes that the slow translocation of the sugar (phlorizin) binding site on the carrier from a predominant inward- to an outward-facing configuration is responsible for the slow kinetics of phlorizin binding to this newly available site [2, 59]. Alternatively, then, the meaning of the fast-acting slow-binding paradigm was confronted with the predictions of the three relevant mechanisms whereby the inhibitor binding step either represents (A), precedes (B), or follows (C) the rate-limiting step in a binding reaction [20]. It was demonstrated in these studies that the recruitment hypothesis, which is formally equivalent to mechanism C above, cannot apply to SGLT because of its associated implication that equilibrium binding of phlorizin should be reached within the subsecond time range to account for the turnover number of 5–125 catalytic cycles per second currently documented for the SGLT1 protein under a large spectrum of experimental conditions [29].

The present studies thus aimed at reevaluating the kinetics of phlorizin binding to, and dissociation from rabbit renal BBMV isolated from the whole kidney cortex using a fast-sampling rapid-filtration apparatus (FS-RFA [4], US patent # 5,330,717) for uptake measurements. These studies were performed at pH 6.0 and 8.6, which isolate up to 95% of the phlorizin molecule under its HPz and Pz^- forms, respectively. Particular attention was paid at characterizing the multicomponent nature of the binding process, which may also involve very low affinity phlorizin (VLAP) binding sites unrelated to glucose transport [1, 7, 11, 15, 25, 51, 60]. The kinetic data were confronted with the previously established criteria aimed at model discrimination between the A-C mechanisms of inhibitor binding [20]. It is concluded that the HAP binding sites observed in kidney cortex BBMV are homogeneous and characterize phlorizin binding to the SGLT1 protein only. Moreover, phlorizin binding is a two-step process of the B-type whereby the rapidly formed initial collision complex is lost during binding measurements by the rapid filtration technique whereas the slowly isomerizing complex is stabilized by the Na^+ ions such that the phlorizin molecule is occluded within its receptor sites on the protein.

Materials and Methods

Materials

Rabbits were purchased from the "Ferme de Sélection Cunipur" (St-Valérien, Québec). [Phenyl-3,3′,5,5′-^{3}H, propanone-3-^{3}H]-phlorizin (specific activity 47.6 Ci/mmol) and D-[1-^{3}H(N)]-glucose (specific activity 10–15 Ci/mmol) were supplied by New England Nuclear (NEN), the BCA (bicinchoninic acid) protein assay kit by Pierce, unlabeled D-glucose by Sigma, phlorizin and ultrapure salts by Aldrich, and amiloride hydrochloride and scintillation cocktail (Beta-Blend) by ICN Biomedicals. Cellulose nitrate filters (12.5 mm diameter, 0.65 μm pore size) were obtained from Micro Filtration Systems (MFS). All other chemicals were of the highest purity available.

Absorption Spectra of Phlorizin

The absorption spectra of phlorizin, resuspended in 50 mM of the appropriate buffers (MES-Tris at pH 5.5–6.5, HEPES-Tris at pH 6.5–8.0, and Tris-MES at pH 8.0–9.5) containing 0.1 mM $MgSO_4$, 300 mM mannitol, and 150 mM NaCl, were recorded on a Shimadzu UV-160 spectrophotometer by varying the wavelength from 250 to 350 nm. As observed previously [18, 34, 54], the absorption maximum shifted from 285 nm at pH 5.5 to 320 nm at pH 9.5. Absorption spectra recorded at phlorizin concentrations of 5, 10, and 20 μM allowed us to determine a mean pK_a value of 7.31 ± 0.04 from which it can be calculated that 95% of the phlorizin is segregated to HPz at pH 6.0 and to Pz^- at pH 8.6.

Preparation of Rabbit Renal BBMV

Renal BBMV were prepared from the whole kidney cortex of male, 2.0–2.5 kg New Zealand white rabbits as described previously [44].

The P_2 and P_4 fractions were resuspended in 50 mM Tris-MES (pH 8.6), HEPES-Tris (pH 7.0), or MES-Tris (pH 6.0) buffers containing 0.1 mM $MgSO_4$, 300 mM mannitol, and either 200 mM KI or 50 mM KI plus 150 mM NaI for Na^+-free or Na^+-equilibrium conditions, respectively. To insure stability of the preparations over the course of the experiments, 45 μl aliquots of BBMV were frozen in liquid N_2 until the time of assay [10, 41]. The protein concentration of these frozen vesicles was 28–35 mg/ml as estimated with the BCA assay kit using bovine serum albumin as a standard.

Phlorizin Binding Assays

Phlorizin binding was determined at 20°C using the automated FSRFA developed in our laboratory [4] as follows. For each assay, 40 μl of BBMV were thawed, prewarmed, and loaded into the apparatus. Binding was initiated by injecting the vesicles into 960 μl of the appropriate media: 50 mM Tris-MES (pH 8.6) or MES-Tris (pH 6.0) buffers containing 0.1 mM $MgSO_4$, 0.5 mM amiloride, 300 mM mannitol or 100 mM mannitol plus 200 mM D-glucose, 0.1 μM ^{3}H-phlorizin in the presence or absence of added unlabeled phlorizin concentrations (0.1, 0.4, 1, 2, 5, 10, 20, 50, 100, 200, 500, and 1000 μM), and either 200 mM KI or 50 mM KI plus 150 mM NaI for Na^+-free or Na^+-equilibrium conditions, respectively. Five time course studies, consisting in 18-point automatic sequential sampling (50 μl) of the above mixture up to 400 sec, were performed at each phlorizin concentration. Samples were injected into 1 ml of ice-cold stop solution composed of 50 mM MES-Tris (pH 6.0) or Tris-MES (pH 8.6) buffers containing 0.1 mM $MgSO_4$, 300 mM mannitol, and 200 mM of either NaCl or KCl for Na^+- or K^+-equilibrium conditions, respectively. In some experiments, the efficacy of the Na^+-free and Na^+-containing stop solutions at revealing Na^+-dependent phlorizin binding was also compared. The stopped mixture was filtered through 0.65 μm cellulose nitrate filters, and the filters were washed three times with 1 ml of ice-cold stop solution [4]. Phlorizin uptake was then determined by liquid scintillation counting as described previously [10].

Effect of Phlorizin, Glucose, and Na^+ on the Dissociation Rates of Tracer Phlorizin at pH 8.6

The following studies were performed at room temperature (22–24°C) and at pH 8.6 to avoid the contribution to efflux of the VLAP sites that are also present at pH 6.0 (*see* Figs. 3–5).

In the first series of experiments, binding of 0.1 μM ^{3}H-phlorizin was initiated as described under "phlorizin binding assays" for Na^+-equilibrium conditions, except that the reaction was started in 1 ml Eppendorf tubes and that the incubation medium contained either 0, 3, 12, or 1,000 μM unlabeled phlorizin. Following a 10 min incubation period over which equilibrium binding of phlorizin is completed (*see* Fig. 1), the mixture was introduced into the incubation chamber of the FSRFA. At time $t = 0$ of the dissociation studies, 60 μl of unlabeled phlorizin or D-glucose, both dissolved in 17% ethanol, was injected into the incubation chamber to get 1 or 200 mM final concentrations of these products, respectively. Tracer phlorizin dissociation was then followed in time by 18-point automatic sequential sampling of the uptake mixture up to 400 sec. At each time point, 50 μl of the uptake mixture was injected into 1 ml of ice-cold stop solution composed of 50 mM Tris-MES buffer (pH 8.6) containing 0.1 mM $MgSO_4$, 300 mM mannitol, and 200 mM NaCl.

In the second series of experiments, binding of 0.1 μM ^{3}H-phlorizin was initiated as described under "phlorizin binding assays" for Na^+-equilibrium conditions. Following a 10 min incubation period, 18 aliquots were sampled at 0.25 sec intervals and recuperated into the manifold array of the FSRFA [4], the upper chamber being filled with 1 ml of 50 mM Tris-MES buffer (pH 8.6) containing 0.1 mM $MgSO_4$, 300 mM mannitol, and either 150, 100, 50, 25 or 0 mM NaCl. The osmolarity and tonicity of this solution were kept constant by varying KCl concentrations to satisfy a total concentration of 200 mM NaCl + KCl.

In both cases, the sequence of filtrations and washes of the samples was performed as described under "phlorizin binding assays" using the appropriate stop solutions, either immediately (first series) or following a delay period of increasing length [4] as indicated in Fig. 7*A* (second series). The remaining amount of bound phlorizin was then determined by liquid scintillation counting as described previously [10].

Glucose Uptake Assays

Na^+-dependent, ^{3}H-D-glucose uptake was determined at 20°C under zero-trans gradient conditions of both ion and substrate using the FSRFA as described previously [44]. Briefly, for each assay, 20 μl of BBMV were thawed, prewarmed, and loaded into the apparatus. Uptake was initiated by injecting the vesicles into 480 μl of the appropriate buffers (MES-Tris at pH 6.0, HEPES-Tris at pH 7.0, and Tris-MES at pH 8.6) containing 0.1 mM $MgSO_4$, 0.5 mM amiloride, 300 mM mannitol, 50 mM KI, 150 mM NaI, and 4 μM tracer D-glucose. For kinetic parameter determinations, 12 concentrations of cold D-glucose were used (0, 0.01, 0.025, 0.05, 0.1, 0.25, 0.5, 1, 2, 5, 10, and 200 mM) and osmolarity was kept constant by varying mannitol concentrations to satisfy a total concentration of 300 mM cold substrate + mannitol. Five time course studies, consisting in 9-point automatic sequential sampling of the uptake mixture (50 μl) at 1 sec intervals [10, 44], were performed at each of these concentrations. Samples were injected into 1 ml of ice-cold stop solution (50 mM of the above buffers containing 0.1 mM $MgSO_4$, 300 mM mannitol, 1 mM phlorizin, and 200 mM NaCl). The stopped mixture was filtered and washed three times with 1 ml of ice-cold stop solution [4, 10, 44]. The substrate content of the vesicles was then determined by liquid scintillation counting as described previously [10]. Initial rates of tracer glucose transport (v_i^*, pmol.sec^{-1}.mg^{-1} protein) were determined over the 1–9 sec time course of the transport assays by linear or polynomial regression analysis as justified previously [10, 44].

Data Analysis

Except where otherwise stated, the kinetics of tracer phlorizin binding (B^*) were fitted to the single exponential function

$$B^* = B_0^* + B_e^* (1 - e^{-k_{obs}t}) \quad (1)$$

in which B_0^* represents the y intercept (time $t = 0$) whereas k_{obs} stands for the first-order rate constant at which equilibrium binding (B_e^*) is reached. Noting that

$$\left[\frac{dB^*}{dt}\right]_{(t=0)} = B_i^* = k_{obs} B_e^* \quad (2)$$

where B_i^* represents the initial rate of phlorizin binding, the following modification of Eq. (1)

$$B^* = B_0^* + \frac{B_i^*}{k_{obs}} (1 - e^{-k_{obs}t}) \quad (3)$$

thus allowed us to directly determine this parameter from the same data.

As shown in previous papers from our group [5, 10, 42], the Michaelis-Menten equation can be modified as follows

$$Q^* = \sum_{j=1}^{n} \frac{Q_{maxj}T}{K_j + S + T} + k_D T \tag{4}$$

when assuming that the nonradioactive substrate (S) acts as an ideal competitive inhibitor of the tracer substrate (T) with regard to tracer binding or transport (Q^*). Note that Eq. (4) postulates the presence of a nonspecific process with apparent proportionality constant k_D working in parallel with n saturating processes, each of these being characterized by its kinetic parameters $Q_{max} = B_{max}$ (maximum binding capacity) or V_{max} (maximum transport rate) and $K = K_d$ (apparent dissociation constant) or K_m (apparent Michaelis constant) in the case of substrate binding or transport, respectively. The one-site ($n = 1$) and two-site ($n = 2$) models were consistently tested throughout this paper and the best model fit to the data, which was evaluated using a previously established strategy aimed at model discrimination [10, 44], is reported in each of the figures and tables. Note that the indices i and e associated with the kinetic parameters of phlorizin binding consistently refer to the initial rate and equilibrium binding data, respectively.

The kinetics of tracer phlorizin dissociation (E^*) were analyzed using the single decay equation

$$E^* = E_0^* e^{-\frac{t}{\tau_{obs}}} + E_\infty^* \tag{5}$$

in which E_0^* stands for the amount of tracer bound at zero-time of the dissociation experiments whereas τ_{obs} represents the time constant at which tracer binding reaches the final steady-state E_∞^* (infinite time of dissociation).

Linear and nonlinear regression analyzes were performed using commercial softwares (Enzfitter, R.J. Leatherbarrow, copyright 1987, Elsevier-Biosoft; P.Fit, copyright 1991, Fig.P Software Corporation, Biosoft). As such, the errors associated with the kinetic parameter values reported in this paper represent the standard errors of regression (SER) on these parameters.

Abbreviations

BBMV, brush-border membrane vesicles; BCA, bicinchoninic acid; FSRFA, fast-sampling, rapid-filtration apparatus; HAG, high affinity glucose; HAP, high affinity phlorizin; HEPES, N-[2-hydroxyethyl]-piperazine-N′-[2-ethanesulfonic] acid; HPz, neutral, *keto*-phlorizin; LAG, low affinity glucose; LAP, low affinity phlorizin; MES, 2-[N-morpholino]ethane-sulfonic acid; Pz^-, negatively charged, *enol*-phlorizin; SD, standard deviation; SER, standard error of regression; SGLT, Na^+-dependent glucose transport (rbSGLT and hSGLT stand for the rabbit and human forms of the SGLT proteins, respectively); SGLT1, cloned intestinal SGLT proteins; SGLT2 and SGLT3, putative clones of the renal-specific SGLT protein; Tris, tris-[hydroxymethyl]-aminomethane; VLAP, very low affinity phlorizin.

Results

Kinetics of Phlorizin Binding at pH 8.6

Representative members of the family of binding time courses generated in the present studies are reported in Fig. 1*A*, from which it can be appreciated that tracer Pz^- binding is a slow process highly sensitive to increasing concentrations of unlabeled phlorizin up to 1 mM. Although not shown for clarity in this figure, the progress of tracer Pz^- binding recorded in the presence of 200 mM D-glucose or in a Na^+-free medium (containing or not either 200 mM D-glucose or 1 mM unlabeled phlorizin) was found to be superimposable onto that observed at 1 mM unlabeled phlorizin. These results thus clearly indicate that Pz^- binding involves both nonspecific and specific, Na^+/glucose cotransport-related binding sites.

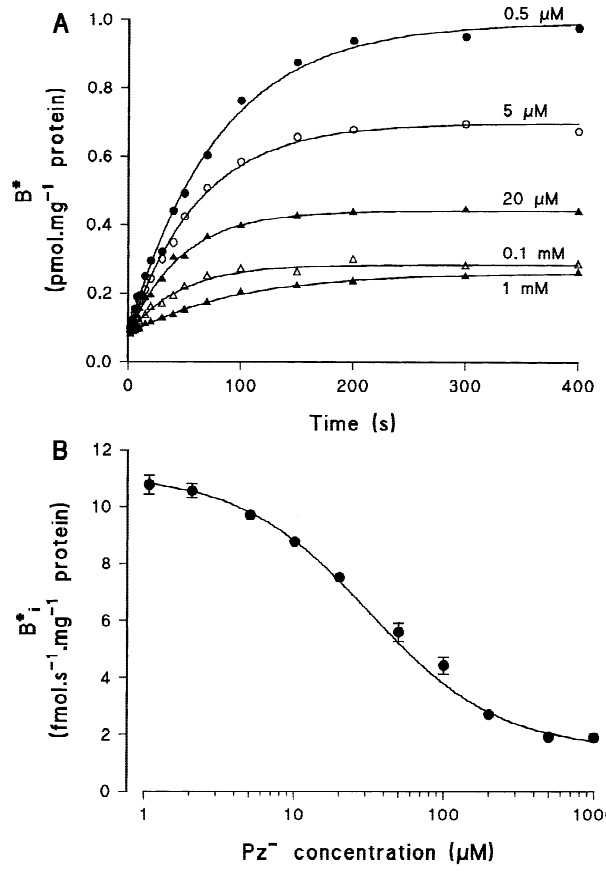

Fig. 1.

As shown in Fig. 1*A*, the kinetics of Pz^- binding are satisfactorily described by single exponential kinetics in which the B_0^* term of Eqs. (1) or (3) proves to be insensitive to unlabeled phlorizin concentrations with mean value of 0.080 ± 0.005 pmol.mg^{-1} protein. These analyses also allow us to establish that the B_i^* (Fig. 1*B*) and B_e^* (Fig. 2*A*, closed circles) data are best compatible with the one-site model, thus indicating in both cases the existence of a single class of Na^+-dependent and D-glucose-sensitive Pz^- binding sites with kinetic parameter values as listed in Table 1. Note that the higher K_{di} than K_{de} values are compatible with the visual inspection of Fig. 1*A*, which clearly shows that the initial rates of tracer Pz^-

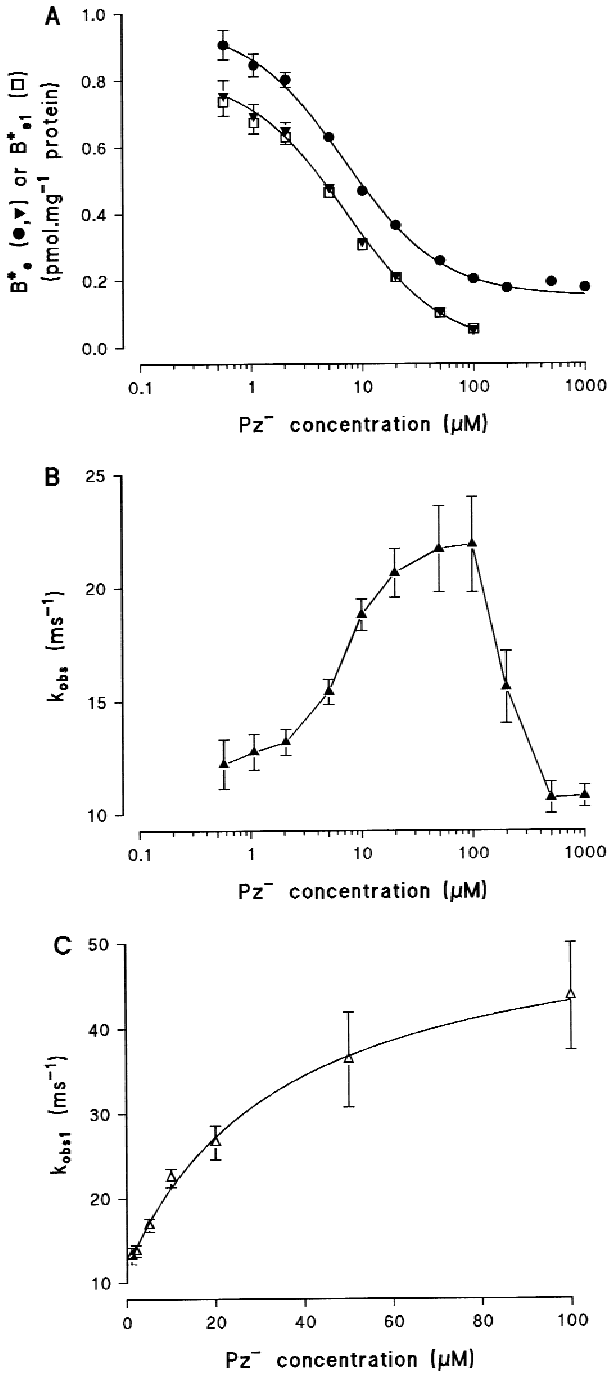

Fig. 2. Concentration-dependence of tracer Pz^- binding at equilibrium (*A*) and of the apparent first-order rate constant at which equilibrium binding is reached (*B* and *C*). Experimental conditions were as described in the legend to Fig. 1. The kinetics of phlorizin binding were fit to Eq. (1) in the text (*see* Fig. 1*A*), in which case the corresponding B_e^*, uncorrected (●) or corrected (▼) for nonspecific binding, and k_{obs} (▲) ± SER values are shown in *A* and *B*, respectively. Alternatively, the kinetics of phlorizin binding were fit to Eq. (6) as described in the text, in which case the corresponding B_{e1}^* (□) and k_{obs1} (△) ± SER values are shown in *A* and *C*, respectively. Lines shown in *A* and *C* are the best-fit curves corresponding to Eqs. (4) and (7) in the text, respectively. Missing error bars in *A* were smaller than the symbol sizes.

Table 1. Kinetic parameters of phlorizin binding at pH 6.0 and 8.6

Kinetic parameters	pH 8.6	PH 6.0
B_{maxi} (pmol.sec^{-1}.mg^{-1} protein)	4.2 ± 0.5	6.8 ± 0.5
K_{di} (μM)	32 ± 4	12.8 ± 1.0
B_{maxe} (pmol.mg^{-1} protein)	78 ± 4	80 ± 5
K_{de} (μM)	7.0 ± 0.5	2.1 ± 0.2
k_{max} (sec^{-1})	0.043 ± 0.003	0.072 ± 0.005
K_m (μM)	34 ± 6	12.9 ± 1.4
k_{min} (sec^{-1})	0.0116 ± 0.0005	0.0146 ± 0.0009

Experimental conditions and analyses were as described in the legends to Figs. 1 and 2 at pH 8.6, and to Figs. 4 and 5 at pH 6.0.

binding are less sensitive to unlabeled phlorizin concentrations than the equilibrium binding values.

The k_{obs} values estimated by the single exponential approach first increase at low Pz^- concentrations to reach a maximum at 50–100 μM phlorizin, and then decrease down to their original values at 0.5–1 mM phlorizin (Fig. 2*B*). The transition from an increasing to a decreasing function occurs at an unlabeled phlorizin concentration that displaces approx. 95% of tracer Pz^- from the HAP binding sites (*see* Fig. 2*A*). Clearly, then, the biphasic behavior of k_{obs} *vs.* Pz^- concentrations reflects the fact that an exact description of the progress curves shown in Fig. 1*A* ought to use the biexponential equation

$$B^* = B_0^* + B_{e1}^*(1 - e^{-k_{obs1}t}) + B_{e2}^*(1 - e^{-k_{obs2}t}) \quad (6)$$

rather than Eq. (1) to account for the contribution to total tracer binding of both the specific (kinetic parameters k_{obs1} and B_{e1}^*) and nonspecific (kinetic parameters k_{obs2} and B_{e2}^*) binding sites. However, it proved impossible to adjust simultaneously the 5 parameters of Eq. (6) to these data. This is so at low and high phlorizin concentrations because the k_{obs1} values, close to the k_{obs} values determined over the lower range of phlorizin concentrations where $B_{e2}^* << B_{e1}^*$ (*see* Fig. 1*A*), are nearly equal to the k_{obs2} values, which can be equated to the k_{obs} values determined at 0.5–1 mM phlorizin where $B_{e1}^* \approx 0$ (*see above*). This is so also in the midrange of Pz^- concentrations where $B_{e1}^* \approx B_{e2}^*$ (*see* Fig. 1*A*) because the expected biexponential behavior will mostly go undetected due to the small differences between the k_{obs1} and k_{obs2} values (*see* Fig. 2*B*). Therefore, Eq. (6) degenerates into Eq. (1) over the whole range of phlorizin concentrations, and a comprehensive description of the kinetic data according to the former equation ought to be done after setting some of the parameters at fixed values. Noting that B_0^*, k_{obs2}, and B_{e2}^* can all be determined from the progress curves at 0.5 and 1 mM phlorizin, the latter approach was thus used to generate a consistent set of B_{e1}^* and k_{obs1} values over the 0.5–100 μM range of phlorizin concentrations.

The validity of this curve-peeling strategy is dem-

onstrated in Fig. 2*A* by showing that the displacement curve constructed from the B^*_{e1} data (open squares) is fully compatible with that previously obtained for B^*_e (solid triangles, B^*_e values corrected for the nonspecific binding component of 0.151 ± 0.004 pmol.mg^{-1} protein). The k_{obs1} data is reported in Fig. 2*C* where it can be appreciated that the apparent rate constant characterizing the kinetics of Pz^- binding to the HAP sites can be fit to the Michaelis-Menten type equation

$$k_{obs1} = k_{min} + \frac{k_{max}(I)}{K_m + (I)} \quad (7)$$

in which k_{min} represents the minimum value of k_{obs1} given by the *y*-intercept, k_{max} stands for the maximum value of the second term on the right-hand side of the equality that would be reached at saturating concentrations of phlorizin (*I*), and K_m is analogous to the Michaelis constant, i.e., $k_{obs1} = k_{min} + 1/2\ k_{max}$ when $(I) = K_m$. The numerical values of the different kinetic parameters above are reported in Table 1 where it can further be appreciated that $K_m = K_{di}$.

Kinetics of Phlorizin Binding at pH 6.0

The main features of HPz binding can be appreciated from the data shown in Fig. 3 reporting tracer phlorizin binding under a typical set of Na^+-equilibrium (A) or Na^+-free (B) conditions in which K^+ was substituted for Na^+. All kinetic data are satisfactorily described by the first-order rate Eq. (1) in which the B^*_0 term proves to be insensitive to the experimental conditions with mean value of 0.30 ± 0.02 pmol.mg^{-1} protein. This analysis also allows us to establish that similar equilibrium levels of 0.89 ± 0.03 and 0.87 ± 0.04 pmol.mg^{-1} protein are reached, respectively, in the Na^+- and K^+-media containing 1 mM unlabeled phlorizin. Note that the steady-state level of HPz binding is higher in the Na^+- (Fig. 3*A*, 5.90 ± 0.09 pmol.mg^{-1} protein) as compared to the K^+- (Fig. 3*B*, 2.70 ± 0.10 pmol.mg^{-1} protein) medium but that similar plateau values of 2.48 ± 0.06 (Fig. 3*A*) and 2.35 ± 0.09 (Fig. 3*B*) pmol.mg^{-1} protein are reached following 400 sec incubation with 200 mM glucose in the former and latter media, respectively. These results thus allow us to conclude that HPz binding is a multicomponent process involving nonspecific binding sites, specific binding sites likely unrelated to D-glucose transport, and D-glucose specific binding sites that may qualify to represent (a) secondary active cotransporter(s) with either loose or strict specificity for Na^+ and H^+.

To further characterize HPz binding, experiments similar to those described in Fig. 1*A* were repeated at pH 6.0 in the K^+-glucose and Na^+-control media (*data not shown*). All binding data also proved to be compatible with single exponential kinetics in which the B^*_0 term of

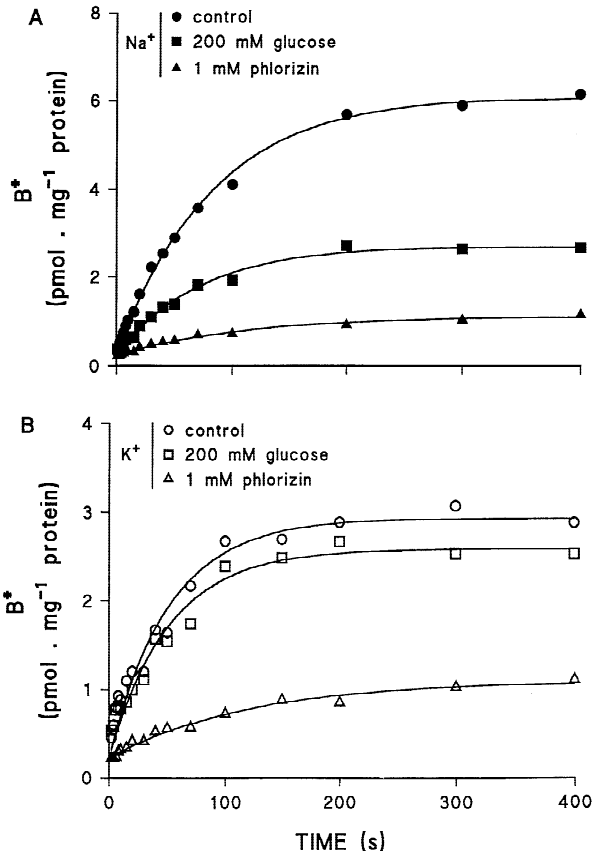

Fig. 3. Kinetics of tracer phlorizin binding at pH 6.0 under Na^+- (*A*) and K^+- (*B*) equilibrium conditions. BBMV were resuspended in 50 mM MES-Tris buffer (pH 6.0) containing 0.1 mM $MgSO_4$, 300 mM mannitol, and either 50 mM KI plus 150 mM NaI (●, ■, ▲) or 200 mM KI (○, □, △). The uptake media were (final concentrations): 50 mM MES-Tris buffer (pH 6.0), 0.1 mM $MgSO_4$, 0.5 mM amiloride, 300 mM mannitol (●, ▲, ○, △) or 100 mM mannitol plus 200 mM D-glucose (■, □), 0.1 μM ^{3}H-phlorizin (●, ■, ○, □) or 0.1 μM ^{3}H-phlorizin plus 1 mM cold phlorizin (▲, △), and either 50 mM KI plus 150 mM NaI (●, ■, ▲) or 200 mM KI (○, □, △). Phlorizin binding was determined at 20°C using the automated FSRFA developed in our laboratory [4]. The reaction was started by injecting 50 μl of BBMV into 950 μl of uptake medium. Lines shown in *A* and *B* are the best-fit curves corresponding to Eq. (1) or its equivalent form Eq. (3) in the text. Each data point represents the mean ± SD of 5 determinations using the same BBMV preparation. Error bars were smaller than the symbol sizes.

Eqs. (1) and (3) was insensitive to unlabeled phlorizin concentrations (mean values of 0.285 ± 0.021 and 0.271 ± 0.060 pmol.mg^{-1} protein in the K^+/glucose and Na^+ media, respectively). Note in Fig. 4*A* that the k_{obs} values estimated in the K^+-glucose medium (open squares) are independent of HPz concentrations (mean value of 13.5 ± 0.8 msec^{-1}). By contrast, those assessed in the Na^+ medium (closed circles) demonstrate a biphasic behavior, first increasing from those seen in the K^+-glucose medium at low HPz concentrations up to a maximum observed at 10–20 μM phlorizin, and decreasing there-

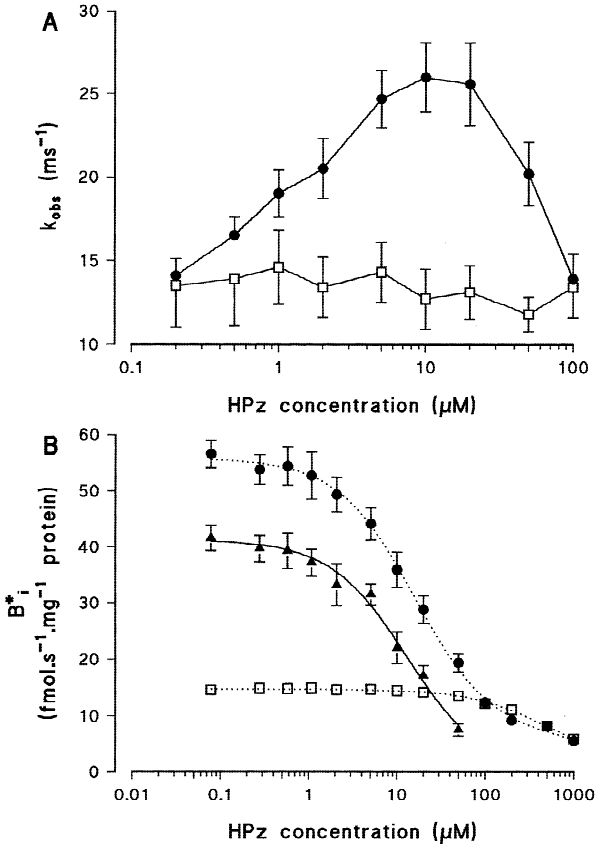

Fig. 4. Concentration-dependence of the apparent first-order rate constant at which equilibrium HPz binding is reached (*A*) and of the initial rates of tracer HPz binding (*B*). Experimental conditions were as described in the legend to Fig. 3 for the K^+-glucose (□) and Na^+-control (●) conditions, except that the incubation medium also contained variable concentrations of unlabeled phlorizin (0.1, 0.4, 1, 2, 5, 10, 20, 50, 100, 200, 500, and 1,000 μM). The kinetics of phlorizin binding were fit to Eq. (3) in the text, and the corresponding k_{obs} and B_i^* ± SER values are shown in *A* and *B*, respectively. In *B*, the B_i^* values recorded in the K^+/glucose medium (□) were subtracted from those estimated in the Na^+ medium (●) to isolate the contribution to total binding of the Na^+-dependent binding sites (▲). The solid line shown in this case is the best-fit curve corresponding to Eq. (4) in the text. Missing error bars were smaller than the symbol sizes.

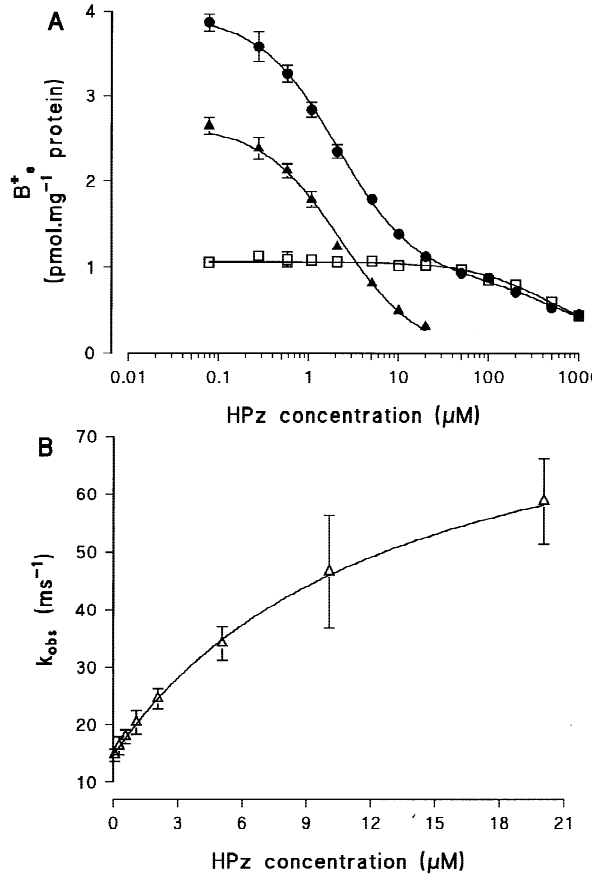

Fig. 5. Concentration-dependence of tracer HPz binding at equilibrium (*A*), and of the apparent first-order rate constant at which HAP equilibrium binding is reached (*B*). Experimental conditions were as described in the legend to Fig. 4. The kinetics of phlorizin binding were fit to Eq. (1) in the text, in which case the B_e^* ± SER values corresponding to the K^+-glucose (□) and Na^+-control (●) conditions are shown in *A*. Missing error bars were smaller than the symbol sizes. Alternatively, the time-dependent contribution of the HAP sites to total binding was isolated by subtracting, at each HPz concentration and at each time point, the *B** values determined in the K^+/glucose medium from those estimated in the Na^+-medium. The resulting data was fit to Eq. (1) in the text, in which case the B_e^* (▲) and k_{obs} (△) ± SER values are shown in *A* and *B*, respectively. Lines shown in *A* are the best-fit curves corresponding to Eq. (4) in the text in which $n = 1$ (□, ▲) or $n = 2$ (●). The line shown in *B* is the best-fit curve corresponding to Eq. (7) in the text.

after down to their original values at 0.1 mM phlorizin. As shown in Fig. 4*B* reporting the initial rates of HPz binding in the Na^+ (closed circles) and K^+/glucose (open squares) media, this biphasic behavior is linked to the saturation of the Na^+-dependent binding sites, which seems to be complete at a phlorizin concentration of 0.1 mM. The lack of saturation of the Na^+-independent binding sites at a phlorizin concentration as high as 1 mM precluded any meaningful extraction of the kinetic parameters from these data. Still, subtracting the B_i^* values recorded in the K^+/glucose medium from those estimated in the Na^+ medium allowed us to isolate the contribution to total binding of the Na^+-dependent binding sites (Fig. 4*B*, closed triangles). These data could then be fit to the one-site model with kinetic parameter values of B_{maxi} and K_{di} as reported in Table 1.

Similarly in Fig. 5*A* reporting the steady-state levels of HPz binding (B_e^*) in the Na^+ (closed circles) and K^+/glucose (open squares) media, saturation of the Na^+-dependent binding sites appears to be complete at 50 μM phlorizin. In the K^+/glucose medium, the B_e^* data are best compatible with the one-site model, thus indicating the existence of a single class of VLAP binding sites (B_{maxe} = 5099 ± 223 pmol.mg^{-1} protein, K_{de} = 443 ±

23 μM) working in parallel with nonspecific binding (0.164 ± 0.007 pmol.mg^{-1} protein, thus similar to that observed at pH 8.6). In the Na^+ medium, the B_e^* data are best compatible with the two-site model and meaningful values of the kinetic parameters (B_{maxe} = 81 ± 6 and 5072 ± 436 pmol.mg^{-1} protein, K_{de} = 2.1 ± 0.2 and 557 ± 66 μM for the HAP and VLAP sites, respectively) can be extracted provided that the apparent k_D value previously observed at pH 8.6 is used as a prompt constant in the fitting routine. Note that the B_{maxe} and K_{de} values estimated for the VLAP sites by this approach are quite comparable to those determined in the K^+/glucose medium. Also, because the K_{de} values characterizing HPz binding to the HAP and VLAP sites differ by more than two orders of magnitude, nearly identical values of the kinetic parameters describing the HAP sites (B_{maxe} = 82 ± 5 pmol.mg^{-1} protein, K_{de} = 2.1 ± 0.2 μM) can be estimated by restricting the analysis of the B_e^* data in the Na^+-medium to the 0.2–20 μM range of phlorizin concentrations. However, the apparent k_D value so determined (10.9 ± 0.4 pmol.mg^{-1} protein.μM^{-1}) now represents the sum B_{maxe}/K_{de} of the VLAP sites (9.1 ± 1.9) + k_D (2.10 ± 0.08) = 11.2 ± 2.0 pmol.mg^{-1} protein.μM^{-1} as obvious from Eq. (4) when $(S + T) << K$.

The time-dependent contribution of the HAP sites to total binding can be isolated by subtracting, at each HPz concentration and at each time point, the B^* values determined in the K^+/glucose medium from those estimated in the Na^+-medium. The resulting data can be fit to Eq. (1) with B_e^* and k_{obs} values as reported in Fig. 5*A* (closed triangles) and *B*, respectively. The B_e^* data in this case is best compatible with the one-site model (B_{maxe} = 76 ± 5 pmol.mg^{-1} protein, K_{de} = 2.2 ± 0.2 μM) whereas the k_{obs} data are best described by Eq. (7) with kinetic parameter values as shown in Table 1. Note in this table that $K_m = K_{di}$ and that $K_{de} < K_{di}$, as was also the case at pH 8.6. However, the K_{de} and K_{di} values estimated at pH 6.0 are both lower than their counterparts previously obtained at pH 8.6 whereas the B_{maxe} and B_{maxi} values recorded at both pH's are comparable (the B_{maxe} and K_{de} values shown at pH 6.0 represent the mean of the different estimates obtained through the different approaches described above).

Dissociation Studies of Pz^- Binding

The first series of experiments, which aimed at evaluating whether the tracer bound phlorizin can exchange rapidly with unlabeled phlorizin or D-glucose, is depicted in Fig. 6 where all efflux data appear satisfactorily described by the single decay Eq. (5). Clearly, the addition of ethanol (Figs. 6*A* and *B*, open circles) leads to slow rates of dissociation (mean τ_{obs} value of 57 ± 5 sec) down to a new steady-state value compatible with tracer dilution alone. Similarly slow dissociation rates, independent of the concentration of tracer bound phlorizin (Fig. 6*A*, mean τ_{obs} value of 66 ± 6 sec), are also observed following the addition of 1 mM unlabeled phlorizin to the BBMV suspension. The dissociation is complete in this case as can be judged from the steady-state plateau values reaching the equilibrium level of nonspecific tracer

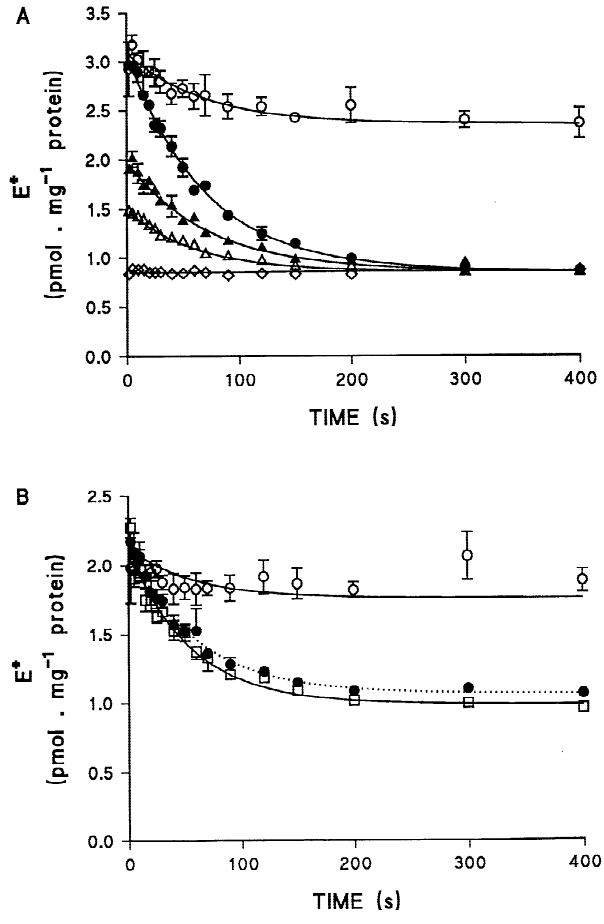

Fig. 6. Kinetics of phlorizin dissociation at pH 8.6 and room temperature. BBMV were resuspended in 50 mM Tris-MES buffer (pH 8.6) containing 0.1 mM $MgSO_4$, 300 mM mannitol, 50 mM KI, and 150 mM NaI. The uptake media contained (final concentrations): 50 mM Tris-MES buffer (pH 8.6), 0.1 mM $MgSO_4$, 0.5 mM amiloride, 300 mM mannitol, 50 mM KI, 150 mM NaI, and 0.08 μM ^{3}H-phlorizin. The reaction was started by mixing 60 μl of BBMV and 940 μl of uptake medium into 1 ml Eppendorf tubes. Following a 10 min incubation period, the mixture was introduced into the incubation chamber of the FSRFA. In *A*, BBMV were preincubated in the presence of either 0 (○, ●), 3 (▲), 12 (△), or 1000 (◇) μM unlabeled phlorizin. Dissociation studies were triggered by the addition of 60 μl of either 17% ethanol (○) or 16.7 mM unlabeled phlorizin dissolved in 17% ethanol (●, ▲, △, ◇). In *B*, BBMV were preincubated in the absence of unlabeled phlorizin. Dissociation studies were triggered by the addition of 60 μl of 17% ethanol (○) or, alternatively, either 3.33 M D-glucose (□) or 16.7 mM unlabeled phlorizin (●) both dissolved in 17% ethanol. Data shown are the mean ± SD of 3 (*B*) or 5 (*A*) experiments performed under each condition. Missing error bars were smaller than the symbol sizes. Curves shown are the best-fit lines to Eq. (5) in the text.

binding recorded at 1 mM unlabeled phlorizin (Fig. 6*A*, open diamonds). The fact that unlabeled phlorizin and D-glucose are both equally inaccessible to the tracer bound phlorizin-receptor complex(es) is quite apparent in Fig. 6*B* where tracer displacement by 1 mM cold phlorizin (closed circles) was also used as an internal control for tracer displacement by 200 mM D-glucose (open squares).

In the next series of experiments reported in Fig. 7, it is demonstrated that phlorizin dissociation from its receptor sites is clearly Na^+-dependent. The dissociation data are compatible with the single decay Eq. (5) in which decreasing τ_{obs} values (increasing rates of dissociation) are observed at decreasing Na^+ concentrations (Fig. 7*A*). Moreover, as shown in Fig. 7*B*, there is a linear relationship between the estimated τ_{obs} values and the Na^+ concentrations used in these experiments. Note in Fig. 7*A* that the rapid rates of phlorizin dissociation in the Na^+-free medium appear to be the main determinant of the low equilibrium values of inhibitor binding recorded under these conditions ($E_0^* = 0.396 \pm 0.058$ *vs.* 1.245 ± 0.018 pmol.mg^{-1} protein in 200 mM KCl *vs.* 150 mM NaCl + 50 mM KCl) because similar infinite time values ($E_\infty^* = 0.483 \pm 0.024$, $n = 6$) are observed under all experimental conditions.

In agreement with these studies, it was found in preliminary experiments that the substitution of KCl for NaCl in the stop solutions led to low equilibrium values of HPz and Pz^- binding independently of whether or not 1 mM unlabeled phlorizin was also present in these solutions.

Kinetic Parameters of Glucose Transport at Various pH Values

The dependence of the initial rates of tracer D-glucose uptake upon increasing cold substrate concentrations was studied at three different pH values (6.0, 7.0, and 8.6) as described in Materials and Methods. All initial rate data were best described by the two-site model (*data not shown*) with kinetic parameter values for the HAG (V_{max1} and K_{m1}) and LAG (V_{max2} and K_{m2}) transport pathways as listed in Table 2. Clearly, K_{m1} and K_{m2} both decrease at increasing pH values. By contrast, V_{max2} is quite insensitive to pH changes whereas V_{max1} demonstrates a biphasic pH dependence, being quite stable between pH 6.0 and 7.0 but decreasing thereafter at pH 8.6. Accordingly, the catalytic efficiency (V_{max}/K_m ratio, expressed as pmol · sec^{-1} · mg^{-1} protein · mM^{-1}) of the HAG transport route first increases from pH 6.0 (163) to pH 7.0 (325) and then decreases at pH 8.6 (179) while that of the LAG transport route continuously increases from pH 6.0 (40) to pH 8.6 (77).

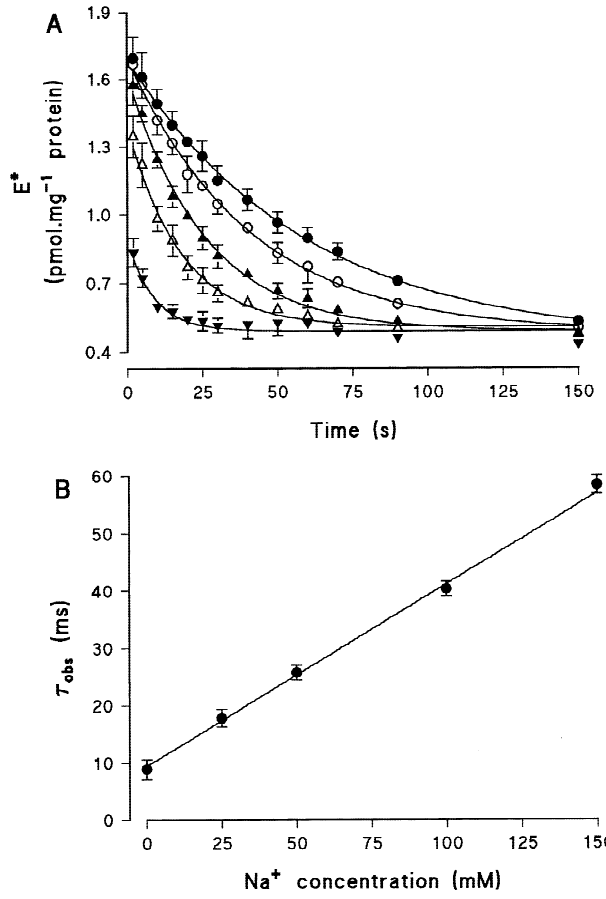

Fig. 7. Effect of Na^+ concentrations on the dissociation rates of Pz^- binding at room temperature. BBMV resuspension and incubation media were as described in the legend to Fig. 6. The reaction was started by injecting 50 μl of BBMV into 950 μl of uptake medium using the automated FSRFA developed in our laboratory [4]. Following a 10 min incubation period, 18 aliquots were sampled at 0.25 sec intervals and recuperated into the manifold array of the FSRFA [4], the upper chamber being filled with 1 ml of 50 mM Tris-MES buffer (pH 8.6) containing 0.1 mM $MgSO_4$, 300 mM mannitol, and either 150 (●), 100 (○), 50 (▲), 25 (△), or 0 (▼) mM NaCl.The osmolarity and tonicity of this solution were kept constant by varying KCl concentrations to satisfy a total concentration of 200 mM NaCl + KCl. The kinetics of Pz^- dissociation are shown in *A* where the data points represent the mean ± SD of 6 experiments performed under each condition. Missing error bars were smaller than the symbol sizes. Lines shown are the best-fit curves to Eq. (5) in the text. The corresponding τ ± SER values are shown in *B* as a function of Na^+ concentrations. The line shown is the best-fit curve obtained by linear regression analysis of the data points.

Discussion

The Three Classes of Phlorizin Binding Sites at Equilibrium

To our knowledge, the present study is the first one that ever tried to characterize the binding kinetics of the *keto* and *enol* forms of phlorizin to renal or intestinal BBMV.

Table 2. Kinetic parameters of glucose transport at various pH values

Kinetic parameters	pH 6.0	pH 7.0	pH 8.6
V_{max1} (pmol.sec^{-1}.mg^{-1} protein)	29.6 ± 8.2	30.9 ± 1.7	9.3 ± 2.0
K_{m1} (μM)	182 ± 38	95 ± 4	52 ± 10
V_{max2} (pmol.sec^{-1}.mg^{-1} protein)	181 ± 64	180 ± 19	207 ± 42
K_{m2} (mM)	4.5 ± 2.9	3.3 ± 0.6	2.7 ± 0.8

BBMV were resuspended in 50 mM MES-Tris (pH 6.0), HEPES-Tris (pH 7.0), or Tris-MES (pH 8.6) buffers containing 0.1 mM $MgSO_4$, 300 mM mannitol, and 200 mM KI. The uptake media contained (final concentrations): 50 mM MES-Tris (pH 6.0), HEPES-Tris (pH 7.0), or Tris-MES (pH 8.6) buffers, 0.1 mM $MgSO_4$, 0.5 mM amiloride, 50 mM KI, 150 mM NaI, 4 μM D-[1-^{3}H(N)]-glucose, and a total of 300 mM mannitol plus added unlabeled D-glucose (0.01, 0.025, 0.05, 0.1, 0.25, 0.5, 1, 2, 5, 10, and 200 mM). Glucose transport was determined at 20°C using the automated FSRFA developed in our laboratory [4]. The reaction was started by injecting 20 μl of BBMV into 480 μl of uptake medium. Initial rates of tracer glucose transport were determined over the 1–9 sec time course of the transport assays by linear or polynomial regression analysis as justified previously [10, 44]. The initial rate data was best-fitted to Eq. (4) in the text with $n = 2$, so that the kinetic parameters V_{max1} and K_{m1} characterize the HAG transport pathway whereas V_{max2} and K_{d2} refer to the LAG transport route.

Altogether, our results identify three main classes of binding sites in rabbit BBMV isolated from the whole kidney cortex. The validity of this conclusion relies on the previous demonstration that glucose transport through the HAG and LAG pathways characterized in this preparation is strictly Na^+-dependent and inhibited competitively by phlorizin [44].

The nonspecific binding sites are best characterized by the insensitivity of tracer phlorizin binding to high concentrations of unlabeled phlorizin (Fig. 1*A*) and similarly contribute to total equilibrium binding at pH 8.6 and 6.0 (0.151 ± 0.004 *vs.* 0.164 ± 0.007 pmol · mg^{-1} in Figs. 2*A* and 5*A*, respectively). The nature of these sites was not investigated further in our study but might be linked to phlorizin partition within the lipid phase of the membrane.

The VLAP binding sites are best characterized by their insensitivity to the presence of glucose (Fig. 3) and/or Na^+ (Figs. 3, 4*B*, and 5*A*) in the uptake media, thus supporting the previous conclusion that these sites are unrelated to glucose transport through the SGLT proteins [1, 7, 11, 15, 25, 51, 60]. The precise nature of the VLAP sites is presently unknown but their apparent homogeneity has been questioned [25]. It was reported in one study that their affinity did not change with temperature [11]; our results further demonstrate that the detection of the VLAP sites is tightly linked to the ionization state of the phlorizin molecule because these sites could only be observed at acidic pH (Fig. 1*A* *vs.* Fig. 3). On this criteria alone, then, the VLAP sites appear homogeneous and might represent phlorizin binding to membrane lipids, as supported by previous studies showing that the neutral form only of phloretin can bind to phosphatidylcholine vesicles [61] and human erythrocyte membranes [22].

Finally, the HAP binding sites are best characterized by their Na^+-dependency and glucose sensitivity (Figs. 1*A* and 3). In this respect, then, the HAP sites do qualify to represent specific binding to (a) cotransport protein(s). This conclusion is compatible with the kinetic mechanisms of cotransport proposed by Wright [64] or Kimmich [29] for SGLT1 and by Mackenzie et al. [39, 40] for SGLT2, all of which share the same essential feature that at least one activator ion must bind to the carrier protein to promote glucose transport and/or phlorizin binding. In this respect, a different conclusion emerged from the studies of Koepsell et al. [30] and Giudicelli et al. [24] in the pig kidney where specific, glucose-sensitive but Na^+-independent phlorizin binding was observed at physiological pH values. These discrepancies may be tentatively resolved from the consideration of species differences or by assuming that the H^+ concentration is still sufficient at pH 7.0 to activate D-glucose cotransport through the SGLT1 protein [26]. Alternatively, because the Na^+ and glucose specificities of phlorizin binding were not systematically investigated under experimental conditions where the HPz and Pz^- forms of phlorizin coexist at neutral pH [24, 30], then the LAP sites observed in these studies might in fact include a significant fraction of the VLAP sites.

Homogeneity of Phlorizin Binding to the HAP Sites

Once corrected for nonspecific phlorizin binding at pH 8.6 and for nonspecific plus VLAP binding at pH 6.0, simple Scatchard kinetics are observed (Figs. 2*A* and 5*A*) with lower apparent affinities of inhibitor binding under initial rate compared to equilibrium conditions (Table 1). These data may indicate some heterogeneity of the HAP sites whereby LAP onset binding and HAP steady-state binding would account for phlorizin binding to the SGLT1 and SGLT2 proteins, respectively [57, 58]. Alternatively, because the kinetics of Pz^- and HPz binding to the HAP sites can be described by single exponential kinetics (Figs. 2*C* and 5*B*) from which the B_e^* and B_i^* data were derived (Figs. 1, 2, 4, and 5), HAP binding may also characterize a two-step process in which a slow isomerization reaction determines the overall rate of inhibitor binding, as previously justified [20].

The second hypothesis could be accounted for by mechanism A whereby phlorizin binding to the transport protein constitutes the rate-limiting step, mechanism B whereby fast phlorizin binding to (an) initial collision complex(es) is followed by a rate-limiting conformation change, or mechanism C whereby phlorizin is titrating (a) carrier conformation(s) in which the receptor bind-

ings sites become slowly accessible to the inhibitor molecules. By contrast to mechanism C, the A and B mechanisms can both generate one (or several) occluded form(s) of the inhibitor-bound receptor complex(es) that are therefore shielded by the rate-limiting step from free exchange with the external milieu. Conversely, most (if not all) of the inhibitor molecules rapidly bound to the initial collision complex(es) in mechanism B or to the accessible carrier species in mechanism C might be lost in any binding assay involving a quench technique to stop the reaction, as occurs with the rapid filtration technique used in the present studies. Therefore, mechanism B can be further subdivided into "B general" (in which all of the inhibitor-bound receptor complexes can be detected) and "B occluded" (in which the occluded complex(es) is (are) the only one(s) that significantly contribute(s) to measured binding.

The confrontation of the kinetic data reported in the present studies with the previously established criteria aimed at model discrimination between the A-C mechanisms of inhibitor binding [20] allows us to set out the following facts. First, the kinetics of Pz^- (Fig. 1*A*) and HPz (Fig. 3) binding are satisfactorily described by Eq. (1) in which the B_0^* term proves to be independent of phlorizin concentrations. This result goes against the predictions of mechanisms C and "B general". Second, the initial rates of HPz and Pz^- binding are compatible with simple Scatchard kinetics (Figs. 1*B* and 4*B*). These results argue against mechanisms A, "B general", and C. Third, the inequality $K_{de} < K_{di}$ observed in Table 1 is a specific property of B mechanisms as compared to mechanisms A and C. Fourth, the apparent first-order rate constant of HPz and Pz^- binding demonstrates a Michaelis-Menten type of dependence on phlorizin concentrations, a property applying to B mechanisms only. Finally, the rate of tracer Pz^- dissociation from its receptor sites is equally insensitive to saturating concentrations of unlabeled phlorizin or D-glucose (Fig. 6*B*), thus showing that the initial collision complex in mechanism "B general" does not contribute to any significant extent to the observed kinetics of binding. Indeed, this situation would result from a fast wash out of the inhibitor molecules bound to this complex during the washing steps in the rapid filtration technique.

Therefore, it can be unambiguously concluded from these data that the kinetics of phlorizin binding to the HAP sites conform to the expectations of mechanism "B occluded". In this respect, the observation in Table 1 that the half-saturation of k_{obs} is achieved at a phlorizin concentration $(I) = K_m = K_{di}$ provides an internal consistency test of this mechanism [20] and supports quite strongly the concept that phlorizin binds to the same cotransport protein under initial rate and equilibrium conditions, thus arguing against the alternative hypothesis of an heterogeneity of the HAP binding sites.

Previous studies from our group [44] demonstrated that phlorizin inhibits the HAG and LAG transport pathways with similar potency in rabbit renal BBMV. It could thus be argued from these data that the proposed homogeneity of the HAP binding sites is only apparent. Yet, Pz^- dissociation from the HAP sites appears to be complete and follows single exponential kinetics with time constant independent of the concentration of tracer-bound phlorizin (Fig. 6*A*). Moreover, the observation that K^+ substitution for Na^+ in the stop solutions reduces quite considerably the detection of steady-state HAP binding at pH 6.0 and 8.6 clearly indicates that phlorizin binding is fully stabilized by Na^+ ions. In support of this view, Fig. 7*A* directly demonstrates that the rate of Pz^- dissociation from the occluded phlorizin-bound receptor complex(es) increases at decreasing Na^+ concentrations in the incubation medium. As Na^+ also proves mandatory for effective formation of the initial collision complex(es) (Figs. 1*A* and 3), it must be inferred from these data that steady-state HAP binding characterizes a cotransport protein whose stoichoimetry of Na^+ and phlorizin binding is higher than the 1:1 coupling ratio usually reported for the SGLT2 protein [28, 39, 40, 58, 65]. We thus conclude that SGLT1 ought to be the sole cotransport protein significantly contributing to HAP binding in rabbit renal BBMV.

Kinetic Model of Phlorizin Binding to the SGLT1 Protein and Validation

No consensus has yet been reached regarding the order of Na^+ (*N*) and substrate (*S*) addition on the SGLT1 protein. The *NNS* model proposed by Parent et al. [45] assumes that the two Na^+ ions bind first in a single reaction step, an hypothesis that has since been shown to be compatible with strong cooperativity for Na^+ binding [19]. By contrast, a *NSN* model whereby *S* binding occurs between the two Na^+ binding events has first been advocated by Kimmich [29] and has since received support from the data of Chen et al. [9]. The demonstration in the present and previous [49] studies that phlorizin dissociation is much faster in the absence than in the presence of Na^+ strongly argues in favor of the *NSN* sequence of substrate addition. Further evidence presented in the previous section also suggests that the last Na^+ ion to bind in mechanism "B occluded" does so at a step following the occlusion of the phlorizin-symporter complex. We therefore propose that phlorizin binding to the SGLT1 protein follows the kinetic scheme depicted in Fig. 8 whereby fast Na^+ and phlorizin binding is followed by a slow conformation change preceding the binding of the second Na^+ ion. As shown in the Appendix, the kinetic equations characterizing this model were derived using a previously described formalism [20] to devise the following consistency tests.

First, the relationships $K_{de} < K_{di}$ and $K_m = K_{di}$ observed in Table 1 and discussed in the previous section are indeed compatible with the proposed model (*see* Eq. [A19], and Eqs. [A14], [A17], and [A18] *vs.* Eq. [A20], respectively). Moreover, the comparison between Eqs. (7) and (A20) allows us to establish that the k_{max} and k_{min} values appearing in Table 1 represent, respectively, the rate constant k_{on} and the apparent rate constant k^*_{off} appearing in this model (*see* Fig. 8 and scheme A1).

Second, using Eq. (A8) and (A19), and remembering that $L_{56} = k_{off}/k_{on}$, it can be demonstrated that the relationship

$$\frac{K_{de}}{K_{di}} = \frac{k^*_{off}}{k_{on} + k^*_{off}} \tag{8}$$

is an intrinsic property of the model depicted in Fig. 8, which appears to be satisfied by the results of the computations reported in Table 3. The following relationships

$$k^*_{off} = \frac{B_{maxi}}{K_{di}} \cdot \frac{K_{de}}{B_{maxe}} \tag{9}$$

$$k_{on} = \frac{B_{maxi}}{B_{maxe}} - k^*_{off} \tag{10}$$

$$k_{on} = k^*_{off}\left[\frac{K_{di}}{K_{de}} - 1\right] \tag{11}$$

can be similarly established from Eq. (A8) and the algebraic expressions of B_{maxe}, K_{de}, B_{maxi}, and K_{di} given by Eqs. (A15)–(A18). Clearly, there is a close agreement between the experimental k_{max} and k_{min} values reported in Table 1, and the calculated k_{on} and k^*_{off} values shown in Table 3.

Last, the kinetic model proposed in Fig. 8 predicts that the apparent time constant τ_{obs} accounting for phlorizin dissociation from its receptor sites should vary linearly with Na^+ concentrations (*see* Eq. [A22]). The data shown in Fig. 7*B* do conform to these expectations and its direct analysis according to Eq. (A22) allows us to establish that $\tau_{off} = 9.4 \pm 0.7$ sec and that $K_{67} = 30 \pm 3$ mM. Note in Fig. 8 that K_{67} represents the intrinsic dissociation constant for binding of the second Na^+ ion to the receptor protein.

These demonstrations thus support quite strongly our conclusion that the HAP sites observed in rabbit renal BBMV characterize phlorizin binding to the SGLT1 protein and validate the proposed mechanism of phlorizin binding to SGLT1 depicted in Fig. 8.

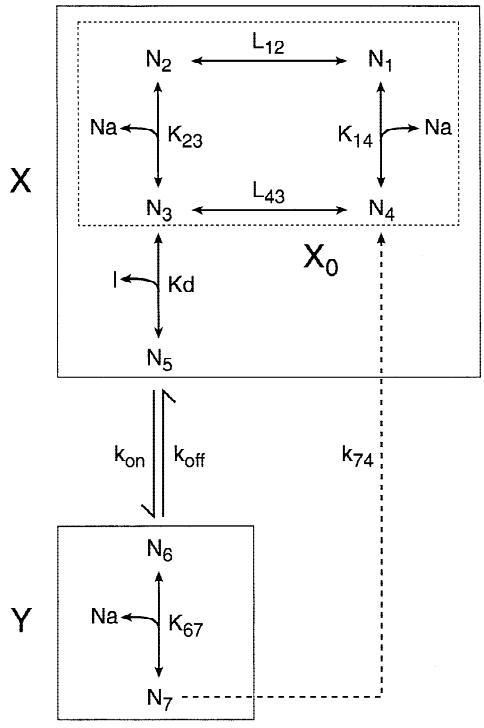

Fig. 8. Kinetic model of phlorizin binding to the SGLT1 protein. For reasons discussed in the text, it is postulated that fast phlorizin (*I*) binding is followed by a rate-limiting isomerization reaction with rate constants k_{on} and k_{off}. This situation is equivalent to stating that all the rate constants governing the association and dissociation of the Na and I effectors with the protein are fast compared to k_{on} and k_{off}. Therefore, it is possible to define two blocks of elementary reactions called *X* and *Y* (full line boxes), in which all the chemical species can be considered to be in equilibrium with each other both before and during the time dependent slow interconversion between blocks *X* and *Y* (*see* the time scale separation hypothesis and the rapid equilibrium assumption previously discussed in [20]). This, in turn, allows us to introduce the dissociation constants L_{12}, K_{14}, K_{23}, L_{43}, K_d, and K_{67} to describe each of the binding and isomerization steps within blocks *X* and *Y*. When applied to the SGLT1 protein for which Na^+ is mandatory for phlorizin binding and stabilizes an occluded conformation of the phlorizin-bound receptor complex (*see* justification in the text), the sequence of elementary reactions involved ought to occur as shown where the N_2 (free carrier), N_3 (Na^+-activated complex), and N_5–N_7 (phlorizin-bound binary and ternary complexes) species stand for the outward-facing conformations of the transport protein whereas N_1 and N_4 represent the inward-facing free carrier and Na^+-activated binary complex, respectively. Moreover, in experiments where BBMV have been resuspended in a Na^+-containing medium, full equilibrium between the N_1–N_4 species prevails at the start of phlorizin addition. Accordingly, it is also possible to define a zero-time block of elementary reactions called X_0 (dashed-line box) from which fast redistribution to the N_1–N_5 species of block X will occur upon phlorizin addition. The dashed line linking the N_7 and N_4 species represents a putative lumped-reaction with rate constant k_{74} that may apply in the case of transported substrates.

Implications of Phlorizin Binding Studies with Regard to the Modelization of Na^+/D-Glucose Cotransport

The present study and previous theoretical considerations from our group [20] invalidate the recruitment concept [2] as a possible explanation of the fast-acting slow-binding paradigm of phlorizin, which can otherwise be resolved by the kinetic scheme depicted in Fig. 8. The fast-acting behavior of phlorizin with regard to its inhibition of glucose transport is readily explained by the

rapid formation of the initial collision complex N_5, thus providing instant competition for glucose binding to the Na^+-activated carrier species N_3. However, because N_5 rapidly dissociates in a rapid filtration assay of phlorizin binding, the slow kinetics of inhibitor binding are only apparent and reflect the (slow) isomerization of this complex into the more stable forms N_6 and N_7. Note that the kinetic scheme depicted in Fig. 8 also reconciles the 1 Na^+:1 phlorizin and the 2 Na^+:1 phlorizin stoichiometries of binding previously observed under initial rate [55] and equilibrium [43, 49] conditions, respectively (*see* Eqs. [A15]–[A18]). Yet, the experiments reported in Fig. 7 rule out the proposal of Semenza's lab [54, 55] that the Na^+-phlorizin-carrier complex may not be functional for the very reason of not binding a second Na^+ ion.

The *NSN* model proposed in Fig. 8 differs from the previous ones [9, 29, 55] by introducing a conformation change consecutive to *S* binding but preceding the attachment of the second Na^+ ion. As a general rule, the isomerization of an intermediary complex that does not involve any substrate addition or product releasing step has no effect on the analytical form of the steady-state rate equations [50], so that the conformation change above would be silent with regard to the kinetics of glucose transport. Still, it can be demonstrated using the computer program of Falk et al. [19] that

$$k_{cat} = \frac{k_{on}k_{74}}{k_{on} + k_{74}} \tag{12}$$

represents a correct expression of the turnover rate of glucose transport for the kinetic mechanism depicted in Fig. 8. Accordingly, the k_{cat} value of 5–125 catalytic cycles per second currently documented for glucose transport through the SGLT1 protein [29] cannot be explained with the small k_{on} (or k_{max}, *see above*) values reported for Pz^- and HPz binding in Table 1 (solving Eq. [12] for k_{74} using the above k_{cat} estimate and the k_{max} values reported in Table 1 leads to negative values of this rate constant). It must be concluded, then, that the kinetics of phlorizin binding represent a "slow-motion movie" of glucose transport, i.e., the conformation change induced by the nontransported inhibitor is far slower than the isomerization step experienced by the transported sugar substrates.

The demonstration that the recruitment concept (mechanism C) is ill-founded at the theoretical [20] and experimental levels (these studies) invalidates the application to phlorizin and the SGLT1 protein of the mathematical derivations proposed by Turner and Silverman [59] to analyze the binding kinetics of nontransported competitive inhibitors. Moreover, the slow isomerization step consecutive to inhibitor binding imposes the condition on a correct interpretation of binding data that a steady-state distribution of the different carrier species involved in the transport cycle, including the rapidly bound phlorizin-carrier complex N_5, has been reached at the time of initial binding measurements. Accordingly, the kinetics of phlorizin binding cannot be related to any putative rate-limiting step in the transport cycle as was done in the past, whether implicitly or explicitly, by Toggenburger et al. [54, 55], Aronson [2], Turner and Silverman [59, 60], Lever [35], and Restrepo and Kimmich [49]. To just give an example with respect to the membrane potential dependency of phlorizin binding observed by a number of authors, it is quite clear that similar results would be expected whether the membrane potential increases the rate of free-carrier recycling [2, 35, 55], the affinity of Na^+ binding to the transport protein [29, 49], or both [45]. This is so because the kinetic mechanism proposed in Fig. 8 states that the initial rate of binding is directly proportional to the concentration of the carrier species onto which phlorizin binds (*see* scheme A1). Accordingly, the algebraic expression of K_{di} explicitly involves the two dissociation constants L_{12} and K_{23} characterizing the free-carrier recycling step and Na^+ binding on the external side, respectively (*see* Eq. [A18]). In fact, this kinetic scheme also suggests a new possibility, namely that the rate constant k_{on} may itself be modulated by the membrane potential, as would seem consistent with the change in the B_{maxi} values (*see* Eq. [A17]) observed in some of the experiments where this parameter was measured [35, 54]. Conversely, the previous demonstration that the membrane potential has no effect on the rate of phlorizin release [2, 49, 55] suggests that both k_{off} and K_{67} are not affected by the electric field.

Finally, the analysis of binding data conforming to the mechanism depicted in Fig. 8 should take into consideration the fact that the kinetic parameters determined under initial rate or equilibrium binding conditions (B_{maxi}, K_{di}, B_{maxe}, and K_{de}, *see* Eqs. [A15]–[A18]) ought to be treated with the same degree of caution as is usually done for their glucose transport counterpart K_m and V_{max}. In this respect, the K_{de} value does not estimate the apparent dissociation constant of phlorizin binding during glucose transport measurements, which is in fact given by K_{di}. In support of this view, the K_{de} values of 2–5 μM (Table 1) agree quite reasonably well with those of approx. 2 μM previously determined at pH 7.4 by Turner and Moran [58] in similar preparations whereas the K_{di} values of 12–30 μM (Table 1) more closely match the K_i value of 15 μM previously reported for phlorizin inhibition of glucose transport [44]. Similarly, the B_{maxe} value does not measure directly the number of receptor binding sites (N_T) and the latter quantity has to be calculated. As shown in Table 3, this can be done in a quite direct way through Eq. (A17) once the k_{on} value has been determined. Alternatively, if the k_{on} and k^*_{off} values are known, N_T can also be calculated from the following relationship,

$$N_T = B_{maxe}\left[1 + \frac{k^*_{off}}{k_{on}}\right] \tag{13}$$

Table 3. Consistency tests of the kinetic model of phlorizin binding to the SGLT1 protein depicted in Fig. 8

Predicted equations	pH 8.6	pH 6.0
Eq. (8): K_{de}/K_{di}	0.21 ± 0.05	0.16 ± 0.03
Eq. (8): $k^*_{off}/(k_{on} + k^*_{off})$	0.22 ± 0.02	0.17 ± 0.02
Eq. (9): $k^*_{off} = (B_{maxi}K_{de})/(B_{maxe}K_{di})$	0.012 ± 0.004	0.014 ± 0.004
Eq. (10): $k_{on} = (B_{maxi}/B_{maxe}) - k^*_{off}$	0.042 ± 0.010	0.070 ± 0.013
Eq. (11): $k_{on} = k^*_{off}[(K_{di}/K_{de}) - 1]$	0.042 ± 0.012	0.075 ± 0.021
Eq. (A17): $N_T = (B_{maxi}/k_{on})$	99 ± 19	94 ± 14
Eq. (13): $N_T = B_{maxe}[1 + (k^*_{off}/k_{on})]$	99 ± 8	96 ± 8

Predicted equations shown refer to those appearing in the main text or appendix. The B_{maxe}, B_{maxi}, K_{de} and K_{di} values used for computation are those reported in Table 1 at each pH. For reasons discussed in the text, the k_{on} and k^*_{off} values used for computation correspond, respectively, to the k_{max} and k_{min} values appearing in Table 1 at each pH.

which can be derived from Eqs. (A15) and (A8) using the relationship $K_{56} = k_{off}/k_{on}$. In the present studies performed at 150 mM Na^+, B_{maxe} thus underevaluates N_T by 20 ± 3 and 27 ± 3% at pH 6.0 and 8.6, respectively. This difference may appear small; however, it should be noted that $0 \leqslant k^*_{off}/k_{on} \leqslant k_{off}/k_{on}$ and that the k^*_{off}/k_{on} ratio $\rightarrow 0$ at saturating Na^+ concentrations (*see* Eq. [A8]), so that the difference would increase at decreasing Na^+ concentrations relative to K_{67}.

HPZ and Pz^- Binding in Relation to the *Keto-Enol* Tautomerism of Phlorizin

The demonstration in Table 3 that HPz and Pz^- bind to the same number of HAP sites departs from the previous suggestion by Toggenburger et al. [54] that the neutral form of phlorizin is the only one to bind to rabbit intestinal BBMV where rbSGLT1 is the sole cotransport protein to be found [10]. However, our observation of lower K_d values at pH 6.0 than pH 8.6 (Table 1) appears fully compatible with the data of these authors showing an increase in the K_i of phlorizin inhibition of SGLT and in the K_d of phlorizin binding at increasing pH values. It can be further argued that the success of Toggenburger et al. [54] at measuring a K_i value relative to phlorizin inhibition of SGLT activity at pH 9.5, i.e., when the inhibitor is segregated to 99% under its ionized Pz^- form, just supports our own data. Similarly, the 2.5- or 3.3-fold difference between the K_{di} or K_{de} values estimated at pH 6.0 *vs.* 8.6 (Table 1) does not support the claim by Lostao et al. [38] that the *enol* form of phlorizin is a much poorer inhibitor of SGLT1 than its *keto* counterpart. This lack of specificity of the SGLT1 protein for HPz *vs.* Pz^- binding contrasts with phloretin, the aglucone moiety of phlorizin (Fig. 9*A*), which interacts with the erythrocyte glucose [22] or anion [21] transport proteins through its neutral or ionized species, respectively. These considerations suggest that different mechanisms are involved in the specific interactions of these two molecules with their relevant receptor proteins.

The early studies of Diedrich [15, 16] and Alvarado [1] suggested that the glucosidic and aglucone moieties of phlorizin (Fig. 9*A*) bind to discrete loci on the transport protein, a characteristic feature that would explain the close to two orders of magnitude difference between the K_d of phlorizin binding and the K_m of glucose transport. However, because this comparison involved the K_d values of phlorizin binding at equilibrium, it would appear in the light of the present studies that the effect of the aglucone site in increasing the affinity of phlorizin relative to glucose has been overestimated in the past. As calculated from Tables 1 and 2, the K_{di} values of HAP binding and the K_{m1} values of HAG transport are separated by factors of 1.6- and 14.2-fold at pH 8.6 and 6.0, respectively. However, these values increase to 7.4- and 87-fold at these same pH if the K_{de} rather than the K_{di} values are used for the comparison.

The molecular modeling studies of Lostao et al. [38] brought evidence that the lowest energy structure for the *keto*-phlorizin conformation places the B-ring in a position such that it folds back over the A and pyranose rings (Fig. 9*A*), similar to a proposed structure for phloretin [22, 61]. This computed structure contrasts with the planar and fully extended conformation of *keto*-phlorizin determined by Cody [12] from the crystal structure of phlorizin (Fig. 9*B*). Note that the latter studies also reported that the overall low energy conformation of HPz was found to be similar to that observed in the crystal structure [12]. Indeed, the symmetry at the 2′- and 6′-positions in phloretin is lost in phlorizin, which could enhance the probability of intramolecular hydrogen bonding between O(9) . . . O(6′) in the latter molecule (Fig. 9*B*). The planar configuration of HPz shown in Fig. 9*B* also contrasts with the L-shaped structure of *enol*-phloretin proposed by Fuhrman et al. [22]. In these molecular modeling studies, it was assumed that the pK_a value of 7.2–7.4, which characterizes the pH-dependent shift in the absorption spectra of phloretin [22] and phlorizin [18, 34, 54, and this study], would represent proton dissociation at the α-position of the *keto* group (Fig. 9*A*). The occurrence of such an enolization mechanism was previously reported for phlorizin [16]. However, much simpler molecules like phloroglucine (Fig. 9*C*) and phlorine (Fig. 9*D*) also demonstrate pH-dependent shifts of similar magnitude [34] whereas 4′-deoxyphlorizin and *para*-phlorizin (4′-glucoside of phloretin) do not [18]. In fact, from the consideration that the latter two molecules are missing the free *para*-phenol group on the A ring (Fig. 9*A*), Evans and Diedrich [18] concluded that it is this proton which is apparently titrated with a pK_a of about 7.2 and not the one at the α-position which undergoes *keto-enol* tautomerization. In this respect, then, the further demonstration by Diedrich [14] that this position

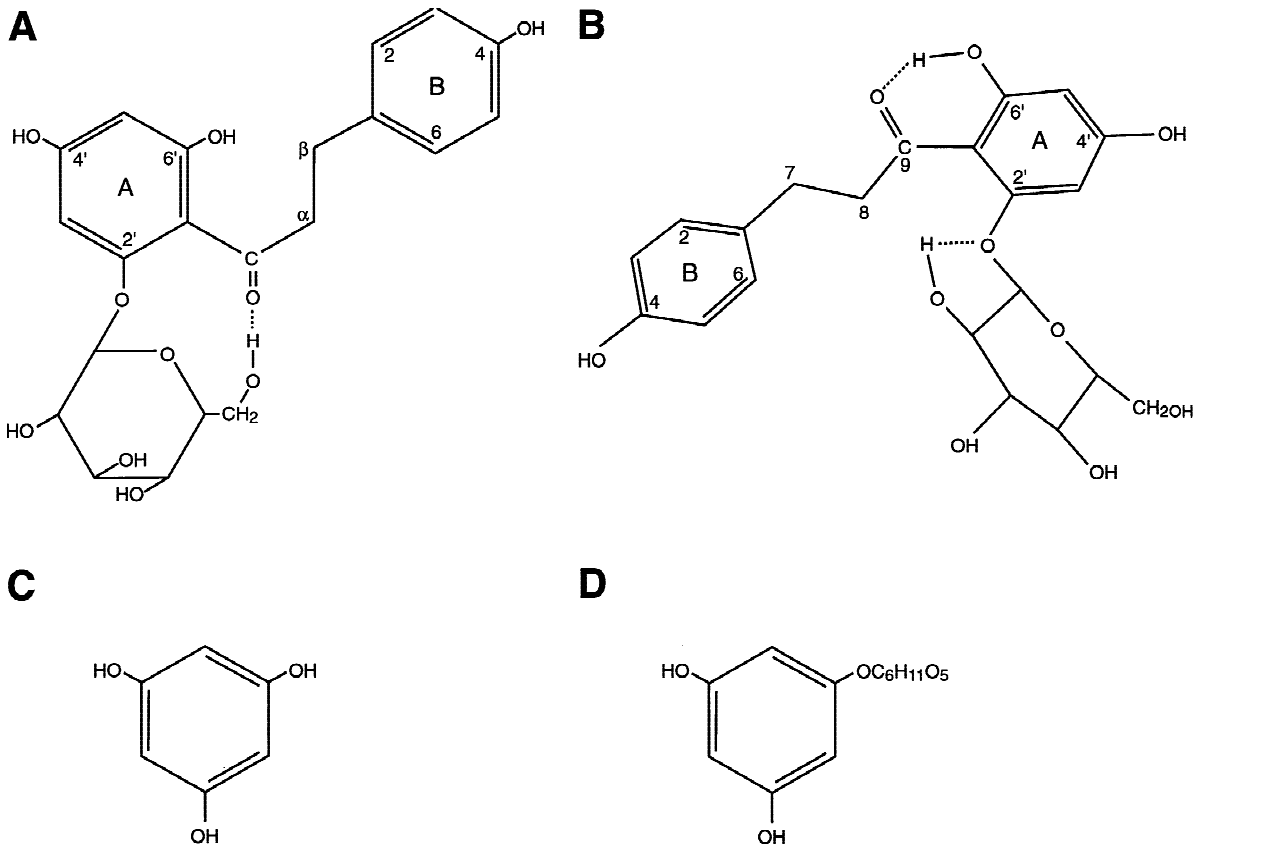

Fig. 9. Phlorizin structures proposed by Diedrich [16] from molecular modeling studies (*A*) and by Cody [12] from crystallographic data (*B*), and chemical structures of phloroglucine (*C*) and phlorine (*D*).

was not critical for activity appears consistent with our own data showing that HPz and Pz^- can both bind to a similar number of transporter sites (Table 3). Notwithstanding the fact that the 3-D structure of the inhibitor and/or the receptor site on the SGLT1 protein can be modified following primary bound formation through its glucose or aglucone moieties, we therefore conclude that major differences in the native 3-D structures of HPz and Pz^- are unlikely to be the main determinant of their affinities for the transport protein.

The interactions of phlorizin with the glucose and aglucone receptor sites likely represent, as suggested by Alvarado [1], a two-step mechanism whereby primary bound formation occurs through either one of these two sites and is followed by secondary attachment to the remaining vacant site. It can be postulated, then, that the rigidity so imposed to the glucose site would impair its occlusion within the glucose channel (decrease the rate of the conformation change), and that extra Na^+ binding would preclude any further reorientation of the transport protein (*see* Fig. 8). In this respect, a different situation is expected when free glucose and free phloretin are bound to the glucose and aglucone sites, respectively, because the rigidity imposed by phlorizin binding to both sites would be lost. Slower transport might be the result, hence the partial noncompetitive nature of phloretin inhibition previously reported by Alvarado [1].

The above random sequence of site occupancy is indeed strongly supported by Alvarado's data [1]. However, the low affinity of the aglucone site for the phloretin molecule would rather suggest that the primary interaction of phlorizin with the SGLT1 protein mostly involves the glycosidic moiety of the inhibitor. This preferred order of site occupancy, also previously suggested by Diedrich [14] and Lostao et al. [38], can be viewed as a B-type mechanism whereby phlorizin binding to the glucose site (dissociation constant K_G) is followed by an isomerization step resulting in the secondary attachment to the phloretin site (dissociation constant K_P), in which case the apparent overall dissociation constant for phlorizin binding (K_d) is given by the quantity $K_G[K_p/(1 + K_P)] < K_G$. Accordingly, the fact that the K_i value for phlorizin inhibition of HAG transport (15 μM in [44]) is smaller than the K_m value for glucose transport through the HAG pathway (100–110 μM in [44]) can be taken as evidence that phlorizin is bound to both of the sugar and aglucone sites during steady-state glucose transport measurements [44]. Moreover, because the K_i and K_{di} values

should be equal under symmetrical conditions of glucose transport and phlorizin binding measurements (*see above*), it also follows from these considerations that phlorizin should be bound to both of the sugar and aglucone sites before the occurence of the slow conformational change depicted in Fig. 8. Therefore, the comparison between the K_{di} and K_{m1} values reported in Tables 1 and 2 suggests that the effect of the aglucone site in increasing the affinity of phlorizin relative to glucose is only marginal at pH 8.6. Moreover, the fact that the K_m of HAG transport increases by 3.5-fold while the K_{di} of HAP binding decreases by 2.5-fold when the pH decreases from 8.6 to 6.0 (Tables 1 and 2) would indicate that the secondary interaction of phlorizin with the aglucone site is specifically increased at acidic pH (assuming that $K_m = K_G$ and $K_d = K_{di}$ in the two-step model described above, then K_P values of 1.6 and 0.076 μM can be estimated at pH 8.6 and 6.0, respectively, so that the affinity of the aglucone site has to increase by 21-fold to compensate for the lower affinity of the glucose site).

The bell-shape dependence on H^+ concentration of the catalytic efficiency of the SGLT1 protein (V_{max1}/K_{m1} ratio, *see* Table 2 and Results) suggests the existence of a minimum of two ionizing groups on the transport protein with pK values of approx. 8.6 and 6.0 (the V_{max1}/K_{m1} ratio decreases by approx. 50% at both pHs). Whereas the former mostly affects V_{max1}, the latter only affects K_{m1} and might well be related to protonation/deprotonation events at or near the glucose binding site. In this respect, the nature of the protein locus involved in phlorizin binding is currently unknown but, according to Dietrich [14], should be one which can donate hydrogen to form a bond with O(4) in the B ring system of the inhibitor molecule (Fig. 9*A*). Accordingly, deprotonation of the aglucone site at more basic pH would impair phlorizin binding, and lower apparent affinity would be the result. Still, this picture does not fit well with the observation that phlorizin derivatives showing lower or higher pK values than the parent molecule exhibit, respectively, lower or similar inhibitory potencies relative to glucose transport at neutral pH [37]. Phlorizin binding may also involve, then, unfavorable electrostatic interactions at basic pH and/or additional molecular features of the inhibitor and receptor sites.

Heterogeneity of Glucose Transport *Vs.* Homogeneity of Phlorizin Binding

Our conclusion that HAP binding observed in rabbit renal BBMV characterizes phlorizin binding to the SGLT1 protein does not question the molecular heterogeneity of renal SGLT, which is indeed strongly supported by the consideration of the clinical findings associated with intestinal glucose/galactose malabsorption and renal glycosuria [13]. However, it does question the concept that the kinetic heterogeneity of glucose transport observed in the proximal tubule reflects the coexpression of distinct SGLT1 and SGLT2 gene products rather than two different transport modes through a unique SGLT1 protein.

The relevance of the latter assertion is clearly restricted by the fact that phlorizin inhibition of the HAG and LAG transport routes can be observed under steady-state conditions of glucose transport measurement [44], thus showing that phlorizin acts as a fast-acting inhibitor on these processes [20]. Therefore, if we assume that the LAG pathway does represent the expression of rbSGLT2 in rabbit renal BBMV and that similar mechanisms of phlorizin binding apply to rbSGLT1 and rbSGLT2, then Na^+-stabilization of phlorizin binding to rbSGLT2 should not be expected for obvious stoichiometric reasons (*see* discussion above in the case of rbSGLT1). Accordingly, the rapid filtration assay used in the present and other studies [1, 7, 11, 15, 18, 24, 25, 30, 51, 54, 55, 60] may not allow us to detect the inhibitor molecules bound onto this transport protein.

Having said this, it is nonetheless true that the HAG and LAG pathways demonstrate a number of overlapping characteristics among which the lack of glucose *vs.* galactose specificities [44] and the similar sensitivities with regard to phlorizin inhibition [44] prove inconsistent with the classical view of glucose transport through the SGLT1 and SGLT2 gene products [13, 57, 58]. Moreover, when estimated from the V_{max} of the HAG pathway at 25°C (41 ± 6 pmol $\cdot$ sec^{-1} $\cdot$ mg^{-1} protein at pH 7.0 in [44]) and the total number of phlorizin binding sites estimated in the present studies (mean value of 97 pmol $\cdot$ mg^{-1} protein from Table 3), the calculated k_{cat} value of 0.42 sec^{-1} is at least one order of magnitude lower than currently documented for glucose transport through the SGLT1 protein [29]. In this respect, then, it may prove significant that the k_{cat} value falls within the expected range (5.8 sec^{-1}) when the combined V_{max} values of the HAG and LAG pathways are instead considered (565 ± 55 pmol $\cdot$ sec^{-1} $\cdot$ mg^{-1} protein in [44]). These simple calculations thus seem to corroborate the concept that the HAG and LAG pathways may not be as fully independent as would have been expected from the coexpression of the SGLT1 and SGLT2 proteins in the same vesicle preparation [57, 58].

The above issues do not resolve the nature of the HAG and LAG pathways, and any attempt to answer this question may only be speculative at this time for two main reasons. First, no consensus has yet been reached regarding the question of which of the putative SGLT2 clones most likely represents the renal SGLT2 protein. In this respect, both Hu14/hSGLT2 [28] and rat SGLT2 [65] mRNA were localized to early proximal tubule cells (S1 segment). However, it was also suggested that the former clone might not represent a SGLT protein because of its substantial evolutionary distance from the

established SGLTs [48]. Similarly, the expression of SAAT1-pSGLT2 mRNA (SGLT3) was reported to be strong in intestine, spleen, liver, and muscle but low in kidney [32], and, to our knowledge, the localization of the SGLT3 protein along the nephron has yet to be established. Moreover, SGLT3 was cloned from the pig kidney cell line LLC-PK_1 [32] showing functional differentiation patterns of proximal tubule cells [36, 46] but hormonal sensitivity which resembles to some extent that of the medullary thick ascending loop [27]. This ambiguity as to the tissular origin of LLC-PK_1 cells is underscored by the reported evidence of SGLT activity in dog distal thick ascending limbs [63]. Second, no consensus has yet been reached regarding the question of the monomeric *vs.* polymeric structure of SGLT1. In this respect, recent evidence suggests that the SGLT1 clone is functionally expressed as a monomeric protein when injected into *Xenopus* oocytes [17]. By contrast, in native intestinal and renal BBMV, the concept of a polymeric structure of SGLT1 is strongly supported by inactivation radiation [3, 52, 53, 56] as well as other studies [6, 10, 23, 30, 31, 44]. It is quite possible, then, that the kinetic heterogeneity of glucose transport observed in the kidney cortex reflects the existence of two different states of aggregation of the same SGLT1 protein in the proximal tubule cells, maybe due to the presence of a kidney specific protein that interacts with the SGLT1 protein in some of these cells as also suggested by other workers in the field [24, 31, 33, 47, 62].

The authors thank C. Gauthier for the art work. The technical assistance of Mrs. C. Leroy has been greatly appreciated. N.O. was supported by a fellowship from the GRTM. This research was supported by grant MT-14407 from the Medical Research Council of Canada.

References

1. Alvarado, F. 1967. Hypothesis for the interaction of phlorizin and phloretin with membrane carriers for sugars. *Biochim. Biophys. Acta* **135:**483–495
2. Aronson, P. 1978. Energy-dependence of phlorizin binding to isolated renal microvillus membranes. *J. Membrane Biol.* **42:**81–98
3. Béliveau, R., Demeule, M., Ibnoul, K.H., Bergeron, M., Beauregard, G., Potier, M. 1988. Radiation-inactivation studies on brush-border-membrane vesicles. General considerations and application to the glucose and phosphate carriers. *Biochem. J.* **252:**807–813
4. Berteloot, A., Malo, C., Breton, S., Brunette, M. 1991. A fast sampling, rapid filtration apparatus: principal characteristics and validation from studies of D-glucose transport in human jejunal brush-border membrane vesicles. *J. Membrane Biol.* **122:**111–125
5. Berteloot, A., Semenza, G. 1990. Advantages and limitations of vesicles for the characterization and kinetic analysis of transport systems. *Meth. Enzymol.* **192:**409–437
6. Blank, M.E., Bode, F., Baumann, K., Diedrich, D.F. 1989. Computer analysis reveals changes in renal Na^+-glucose cotransporter in diabetic rats. *Am. J. Physiol.* **257:**C385–C396
7. Bode, F., Baumann, K., Diedrich, D.F. 1972. Inhibition of [^{3}H]phlorizin binding to isolated kidney brush border membranes by phlorizin-like compounds. *Biochim. Biophys. Acta* **290:**134–149
8. Cha, S. 1968. A simple method for derivation of rate equations for enzyme-catalyzed reactions under the rapid equilibrium assumption or combined assumptions of equilibrium and steady-state. *J. Biol. Chem.* **243:**820–825
9. Chen, X.-Z., Coady, M., Jalal, F., Wallendorf, B., and Lapointe, J.-Y. 1997. Sodium leak pathway and substrate binding order in the Na^+-glucose cotransporter. *Biophys. J.* **73:**2503–2510
10. Chenu, C., Berteloot, A. 1993. Allosterism and Na^+-D-glucose cotransport kinetics in rabbit jejunal vesicles: compatibility with mixed positive and negative cooperativities in a homo-dimeric or tetrameric structure and experimental evidence for only one transport protein involved. *J. Membrane Biol.* **132:**95–113
11. Chesney, R., Sacktor, B., Kleinzeller, A. 1974. The binding of phlorizin to the isolated luminal membrane of the renal proximal tubule. *Biochim. Biophys. Acta* **332:**263–277
12. Cody, V. 1986. Crystal structure of phlorizin and its interactions in the deiodinase active-site model. *In:* Plant flavonoids in Biology and Medicine: Biochemical, Pharmacological, and Structure-Activity Relationships. pp. 383–386. Alan R. Liss
13. Desjeux, J.-F. 1995. Congenital selective Na^+, D-glucose cotransport defect leading to renal glucosuria and congenital selective intestinal malabsorption of glucose and galactose. *In:* The Metabolic Basis of Inherited Diseases. C.R. Scriver, editor. pp. 3563–3580. McGraw-Hill, New York
14. Diedrich, D.F. 1963. The comparative effects of some phlorizin analogs on the renal reabsorption of glucose. *Biochim. Biophys. Acta* **71:**688–700
15. Diedrich, D.F. 1966. Competitive inhibition of intestinal glucose transport by phlorizin analogs. *Arch. Biochem. Biophys.* **117:**248–256
16. Diedrich, D.F. 1968. Is phloretin the sugar transport inhibitor in intestine? *Arch. Biochem. Biophys.* **127:**803–812
17. Eskandary, S., Wright, E.M., Kreman, M., Starace, D.M., Zampighi, G.A. 1998. Structural analysis of cloned plasma membrane proteins by freeze-fracture electron microscopy. *Proc. Natl. Acad. Sci. USA* **95:**11235–11240
18. Evans, J.O., Diedrich, D.F. 1980. The affinity of phlorizin-like compounds for a β-glucosidase in intestinal brush borders: comparison with the glucose transport system. *Arch. Biochem. Biophys.* **199:**342–348
19. Falk, S., Guay, A., Chenu, C., Patil, S.D., Berteloot, A. 1998. Reduction of an eight-state mechanism of cotransport to a six-state model using a new computer program. *Biophys. J.* **74:**816–830
20. Falk, S., Oulianova, N., Berteloot, A. 1999. Kinetic mechanisms of inhibitor binding: relevance to the fast-acting slow-binding paradigm. *Biophys. J.* **77:**173–188
21. Forman, S.A., Verkman, A.S., Dix, J.A., Solomon, A.K. 1982. Interaction of phloretin with the anion transport protein of the red blood cell membrane. *Biochim. Biophys. Acta* **689:**531–538
22. Fuhrmann, G.F., Dernedde, S., Frenking, G. 1992. Phloretin *keto-enol* tautomerism and inhibition of glucose transport in human erythrocytes (including effects of phloretin on anion transport). *Biochim. Biophys. Acta* **1110:**105–111
23. Gerardi-Laffin, C., Delque-Bayer, P., Sudaka, P., Poirée, J.C. 1993. Oligomeric structure of the sodium-dependent phlorizin binding protein from kidney brush-border membranes. *Biochim. Biophys. Acta* **1151:**99–104
24. Giudicelli, J., Bertrand, M.-F., Bilski, S., Tran, T.T., Poirée, J.-C. 1998. Effect of cross-linkers on the structure and function of pig-renal sodium-glucose cotransporters after papain treatment. *Biochem. J.* **330:**733–736
25. Glossmann, H., Neville, D.M. Jr. 1972. Phlorizin receptors in iso-

lated kidney brush border membranes. *J. Biol. Chem.* **247:**7779–7789
26. Hirayama, B.A., Loo, D.D.F., Wright, E.M. 1994. Protons drive sugar transport through the Na^+/glucose cotransporter (SGLT1). *J. Biol. Chem.* **269:**21407–21410
27. Horster, M.F., Stopp, M. 1986. Transport and metabolic functions in cultured renal tubule cells. *Kidney Int.* **29:**46–53
28. Kanai, Y., Lee, W.S., You, G., Brown, D., Hediger, M.A. 1994. The human kidney low affinity Na^+/glucose cotransporter SGLT2. *J. Clin. Invest.* **93:**397–404
29. Kimmich, G.A. 1990. Membrane potentials and the mechanism of intestinal Na^+-dependent sugar transport. *J. Membrane Biol.* **114:**1–27
30. Koepsell, H., Fritzsch, G., Korn, K., Madrala, A. 1990. Two substrate sites in the renal Na^+-D-glucose cotransporter studied by model analysis of phlorizin binding and D-glucose transport measurements. *J. Membrane Biol.* **114:**113–132
31. Koepsell, H., Spangenberg, J. 1994. Function and presumed molecular structure of Na^+-D-glucose cotransport systems. *J. Membrane Biol.* **138:**1–11
32. Kong, C-T., Yet, S.-F., Lever, J.E. 1993. Cloning and expression of a mammalian Na^+/amino acid cotransporter with sequence similarity to Na^+/glucose cotransporters. *J. Biol. Chem.* **268:**1509–1512
33. Lambotte, S., Veyhl, M., Kohler, M., Morrison-Shetlar, A.I., Kinne, R.K., Schmid, M., Koepsell, H. 1996. The human gene of a protein that modifies Na^+-D-glucose cotransport. *DNA Cell Biol.* **15:**769–777
34. Lambrechts, A. 1937. Contribution à l'étude chimique et physicochimique de la phlorizine et de quelques substances voisines. *Arch. Int. Physiol.* **44:**4–39
35. Lever, J.E. 1984. A two sodium ion/D-glucose symport mechanism: Membrane potential effects on phlorizin binding. *Biochemistry* **23:**4697–4701
36. Lever, J.E. 1986. Expression of differentiated functions in kidney epithelial cell lines. *Miner. Electrol. Metab.* **12:**14–19
37. Lin, J.T., Hahn, K.-D., Kinne, R. 1982. Synthesis of phlorizin derivatives and their inhibitor effect on the renal sodium/D-glucose cotransport system. *Biochim. Biophys. Acta* **693:**379–388
38. Lostao, M.P., Hirayama, B.A., Loo, D.D.F., Wright, E.M. 1994. Phenylglucosides and the Na^+/glucose cotransporter (SGLT1): analysis of interactions. *J. Membrane Biol.* **142:**161–170
39. Mackenzie, B., Loo, D.D.F., Panayotova-Heiermann, M., Wright, E.M. 1996. Biophysical characteristics of the pig kidney Na^+/glucose cotransporter SGLT2 reveal a common mechanism for SGLT1 and SGLT2. *J. Biol. Chem.* **271:**32678–32683
40. Mackenzie, B., Panayotova-Heiermann, M., Loo, D.D.F., Lever, J.E., Wright, E.M. 1994. SAAT1 is a low affinity Na^+/glucose cotransporter and not an amino acid transporter. *J. Biol. Chem.* **269:**22488–22491
41. Maenz, D.D., Chenu, C., Bellemare, F., Berteloot, A. 1991. Improved stability of rabbit and rat intestinal brush border membrane vesicles using phospholipase inhibitors. *Biochim. Biophys. Acta* **1069:**250–258
42. Malo, C., Berteloot, A. 1991. Analysis of kinetic data in transport studies: new insights from kinetic studies of Na^+-D-glucose cotransport in human brush-border membrane vesicles using a fast sampling, rapid filtration apparatus. *J. Membrane Biol.* **122:**127–141
43. Moran, A., Davis, L.J., Turner, R.J. 1988. High affinity phlorizin binding to the LLC-PK_1 cells exhibits a sodium:phlorizin stoichiometry of 2:1. *J. Biol. Chem.* **263:**187–192
44. Oulianova, N., Berteloot, A. 1996. Sugar transport heterogeneity in the kidney: two independent transporters or different transport modes through an oligomeric protein? 1. glucose transport studies. *J. Membrane Biol.* **153:**181–194
45. Parent, L., Supplisson, S., Loo, D.D.F., Wright, E.M. 1992. Electrogenic properties of the cloned Na^+/glucose cotransporter: II. A transport model under nonrapid equilibrium conditions. *J. Membrane Biol.* **125:**63–79
46. Rabito, C.A. 1986. Sodium cotransport processes in renal epithelial cell lines. *Miner. Electrol. Metab.* **12:**32–41
47. Reinhardt, J., Veyhl, M., Wagner, K., Gambaryan, S., Dekel, C., Akhoundova, A., Kom, T., Koepsell, H. 1999. Cloning and characterization of the transport modifier RS1 from rabbit which was previously assumed to be specific for Na^+-D-glucose cotransport. *Biochim. Biophys. Acta* **1417:**131–143
48. Reizer, J., Reizer, A., Saier, M.H. Jr. 1994. A functional superfamily of sodium/solute symporters. *Biochim. Biophys. Acta* **1197:**133–166
49. Restrepo, D., Kimmich, G.A. 1986. Phlorizin binding to isolated enterocytes: Membrane potential and sodium dependence. *J. Membrane Biol.* **89:**269–280
50. Segel, I.H. 1975. Steady-state kinetics of multireactant enzymes. *In:* Enzyme kinetics: behavior and analysis of rapid equilibrium and steady-state enzyme systems. J. Wiley & Sons, editor. Chap. 9, pp. 505–845. Wiley-Interscience, New-York
51. Silverman, M., Black, J. 1975. High affinity phlorizin receptor sites and their relation to the glucose transport mechanism in the proximal tubule of dog kidney. *Biochim. Biophys. Acta* **394:**10–30
52. Stevens, B.R., Fernandez, A., Hirayama, B., Wright, E.M., Kempner, E.S. 1990. Intestinal brush border membrane Na^+/glucose cotransporter functions in situ as a homotetramer. *Proc. Natl. Acad. Sci. USA* **87:**1456–1460
53. Takahashi, M., Malathi, P., Preiser, H., Jung, C.Y. 1985. Radiation inactivation studies on the rabbit kidney sodium-dependent glucose transporter. *J. Biol. Chem.* **260:**10551–10556
54. Toggenburger, G., Kessler, M., Rothstein, A., Semenza, G., Tannenbaum, C. 1978. Similarity in effect of Na^+ gradient and membrane potentials on D-glucose transport by, and phlorizin binding to, vesicles derived from brush borders of rabbit intestinal mucosal cells. *J. Membrane Biol.* **40:**269–290
55. Toggenburger, G., Kessler, M., Semenza, G. 1982. Phlorizin as a probe of the small intestinal Na^+, D-glucose cotransporter. A model. *Biochim. Biophys. Acta* **688:**557–571
56. Turner, R.J., Kempner, E.S. 1982. Radiation inactivation studies of the renal brush-border membrane phlorizin-binding protein. *J. Biol. Chem.* **257:**10794–10797
57. Turner, R.J., Moran, A. 1982. Heterogeneity of sodium-dependent D-glucose transport sites along the proximal tubule: evidence from vesicle studies. *Am. J. Physiol.* **242:**F406–F414
58. Turner, R.J., Moran, A. 1982. Stoichiometric studies of the renal outer cortical brush border membrane D-glucose transporter. *J. Membrane Biol.* **67:**73–80
59. Turner, R.J., Silverman, M. 1980. Testing carrier models of cotransport using the binding kinetics of nontransported competitive inhibitors. *Biochim. Biophys. Acta* **596:**272–291
60. Turner, R.J., Silverman, M. 1981. Interaction of phlorizin and sodium with the renal brush-border membrane D-glucose transporter: stoichiometry and order of binding. *J. Membrane Biol.* **58:**43–55
61. Verkman, A.S., Solomon, A.K. 1982. A stepwise mechanism for the permeation of phloretin through a lipid bilayer. *J. Gen. Physiol.* **80:**557–581
62. Veyhl, M., Spangenberg, J., Puschel, B., Poppe, R., Dekel, C., Fritzsch, G., Haase, W., Koepsell, H. 1993. Cloning of a membrane-associated protein which modifies activity and properties of the Na^+-D-glucose cotransporter. *J. Biol. Chem.* **268:**25041–25053
63. Vinay, P., Senecal, J., Noël, J., Chirinian, C., Vinay., M.C., Am-

mann, H., Boulanger, Y., Gougoux, A., Berteloot, A. 1991. Basolateral glucose transport in distal segments of the dog nephron. *Can. J. Physiol. Pharmacol.* **69:**964–977

64. Wright, E.M. 1993. The intestinal Na^+/glucose cotransporter. *Annu. Rev. Physiol.* **55:**575–589
65. You, G., Lee, W-S., Barros, E.J.G., Kanai, Y., Huo, T-L., Khawaja, S., Wells, R.G., Nigam, S.K., Hediger, M.A. 1995. Molecular characteristics of Na^+-coupled glucose transporters in adult and embryonic rat kidney. *J. Biol. Chem.* **270:**29365–29371

Appendix

Kinetics of Phlorizin Binding Conforming to the Mechanism Depicted in Fig. 8

It was shown previously [20] that the kinetic mechanism of inhibitor binding depicted in Fig. 8, in which the slow isomerization step linking the N_5 and N_6 species constitutes the overall rate-limiting step in the binding process, can be reduced to scheme (A1)

*Scheme A*1 $\quad X \underset{k_{off}^* = k_{off} f_6}{\overset{k_{on}^* = k_{on} f_5}{\rightleftharpoons}} Y$

according to Cha's formalism [8]. Note that the apparent rate constants k_{on}^* and k_{off}^* linking the *X* and *Y* blocks in Scheme (A1) now replace the true rate constants k_{on} and k_{off} appearing in Fig. 8. The latter are weighted by the factors f_5 and f_6 whose mathematical expressions

$$f_5 = \frac{N_5}{X} = \frac{N_5}{\sum_{j=1}^{5} N_j^X} \tag{A1}$$

$$f_6 = \frac{N_6}{Y} = \frac{N_6}{N_6 + N_7} \tag{A2}$$

clearly indicate that they represent the fractional concentrations of the chemical species N_5 and N_6 within blocks *X* and *Y*, respectively. The denominators of Eqs. (A1) and (A2) can be expressed relative to the N_5 and N_6 species as

$$X = N_5 \left\{ 1 + \frac{K_d}{(I)} \left[1 + L_{43} + \frac{K_{23}}{(Na)} (1 + L_{12}) \right] \right\} \tag{A3}$$

$$Y = N_6 \left[1 + \frac{(Na)}{K_{67}} \right] \tag{A4}$$

in which K_d, L_{12}, L_{43}, and K_{67} represent the dissociation constants of the rapid steps in blocks *X* and *Y* as indicated in Fig. 8. Note that the dissociation constant K_{14} does not appear in Eqs. (A3) and (A4) because the following relationship

$$L_{12} K_{23} = K_{14} L_{43} \tag{A5}$$

applies to the N_1–N_4 cycle. Moreover, the two blocks *X* and *Y* are linked through the conservation equation

$$X + Y = N_T \tag{A6}$$

in which N_T represent the total amount of binding sites.

The following expressions

$$k_{on}^* = k_{on} f_5 = \frac{k_{on}(I)}{K_d \left[1 + L_{43} + \frac{K_{23}}{(Na)} (1 + L_{12}) \right] + (I)} \tag{A7}$$

$$k_{off}^* = k_{off} f_6 = \frac{k_{off} K_{67}}{K_{67} + (Na)} \tag{A8}$$

can thus be established using Eqs. (A1)–(A4) above.

It was previously demonstrated that the interconversion between blocks *X* and *Y* in scheme (A1) can be described by the monoexponential function

$$Y = Y_e (1 - e^{-k_{obs} t}) \tag{A9}$$

in which

$$Y_e = \frac{k_{on}^* N_T}{k_{obs}} \tag{A10}$$

stands for the equilibrium concentrations of *Y* at the end of the relaxation process whereas

$$k_{obs} = k_{on}^* + k_{off}^* \tag{A11}$$

represents the apparent first-order rate of this process [20]. Note that Eq. (A9) makes the following assumptions with regard to the conditions of the binding assay, which all apply to the studies presented in the main text. Firstly, the relevant preparation to be tested for inhibitor binding has been resuspended long enough in the uptake medium to ensure that true equilibrium conditions have been reached with all effector molecules present at the time of the assay, so that it is possible to calculate the boundary conditions (X_{00} and Y_{00}) prevailing before the start of the binding assay. Secondly, the binding assay is started by mixing the above preparations in a medium of identical composition also containing the inhibitor to be tested, so that there will be fast redistribution only of those N_j^X or N_j^Y species involved in rapid equilibrium reactions with the inhibitor. Accordingly, it is possible to calculate the boundary conditions (X_0 and Y_0) prevailing at the very start of the relaxation process when $t = 0$. The boundary conditions applying to the kinetic mechanism of phlorizin binding depicted in Fig. 8

$$X_{00} = X_0 = N_T; \qquad Y_{00} = Y_0 = 0 \tag{A12}$$

can thus be readily established from these two assumptions.

As demonstrated in the main text, the kinetics of phlorizin binding conform to those expected for mechanism B occluded whereby the rapidly formed initial collision complex (N_5 in Fig. 8) does not contribute to any significant extent to the observed kinetics of binding. This occurs because the rates of association and dissociation of the inhibitor are fast compared to k_{on}^* and k_{off}^*, so that the rapid filtration technique used for the binding assay fails to detect most (if not all) of the inhibitor molecules bound to the N_j^X species. If B^* represents the amount of tracer phlorizin molecules bound to its receptor sites on the transport protein, then $B^* = Y$ in the case of the model depicted in Fig. 8 and

$$B^* = B_e^* (1 = e^{-k_{obs} t}) \tag{A13}$$

where B_e^* and k_{obs} are given by Eqs. (A10) and (A11), respectively. The mathematical expression of the initial rate of phlorizin binding

$$B_i^* = k_{obs} B_e^* \tag{A14}$$

can thus be readily obtained from the first derivative of Eq. (A9) at $t =$

0. A few arithmetic manipulations using the relevant equations above are necessary to demonstrate that B^*_e and B^*_i can be cast under the scatchard form of Eq. (4) in text with the following algebraic expressions of the kinetic parameters

$$B_{maxe} = \frac{[K_{67} + (Na)]\, N_T}{K_{67}(1 + L_{56}) + (Na)} \tag{A15}$$

$$K_{de} = \frac{L_{56}K_{67}[K_{23}(1 + L_{12}) + (1 + L_{43})(Na)]}{[K_{67}\,(1 + L_{56}) + (Na)]\,(Na)}K_d \tag{A16}$$

$$B_{maxi} = k_{on}\, N_T \tag{A17}$$

$$K_{di} = \left[1 + L_{43} + \frac{K_{23}}{(Na)}\,(1 + L_{12})\right]K_d \tag{A18}$$

in which $L_{56} = k_{off}/k_{on}$. The comparison of Eqs. A(16) and A(18) allows us to establish that

$$\frac{K_{de}}{K_{di}} = \frac{L_{56}\,K_{67}}{K_{67}\,[1 + L_{56}] + (Na)} \leq 1 \tag{A19}$$

as previously demonstrated for mechanism B [20]. Using Eqs. A(7), A(11) and A(18), it is also possible to demonstrate that

$$k_{obs} = k^*_{off} + \frac{k_{on}\,(I)}{K_{di} + (I)} \tag{A20}$$

which is similar in form to Eq. (7) in the main text with $k_{min} = k^*_{off}$, $k_{max} = k_{on}$, and $K_m = K_{di.}$

Kinetics of Phlorizin Dissociation Conforming to the Mechanism Depicted in Fig. 8

With the experimental protocol used for the experiments described in Fig. 7, it is readily apparent that the kinetics of tracer phlorizin dissociation from its receptor sites on the protein can be described by the differential equation $E^* = -(dB^*_{dt}/dt)$, which can be integrated as

$$E^* = B^*_e\, e^{-k^*_{off}t} + E^*_\infty \tag{A21}$$

where k^*_{off} and B^*_e are given by Eqs. (A8) and (A10), respectively. Note that Eq. (A21) is identical to Eq. (5) in the main text with $\tau_{obs} = 1/k^*_{off}$ and $E^*_0 = B^*_e$. Strictly speaking, the integration constant E^*_∞ appearing in Eq. (A21) should be equal to zero when considering that phlorizin should completely dissociate from its HAP receptor sites. However, this is not so in Eq. (5) because the experimental data appearing in Fig. 7 was not corrected for the contribution to total binding of the non-specific binding sites also present in the BBMV preparation. In any case, the apparent time constant of phlorizin dissociation appearing in Eq. (5) in the main text should be described by

$$\tau_{obs} = \tau_{off}\left[1 + \frac{(Na)}{K_{67}}\right] \tag{A22}$$

as can be computed from the transformation of Eq. (A8) with $1/k_{off} = \tau_{off}$.